1

Device Concept of Transflective Liquid Crystal Displays

1.1 Overview

The ability to electrically tune optical birefringence makes liquid crystal (LC) a useful material for electro-optical applications. Because of its compact size and light weight, liquid crystal displays (LCDs) have been used extensively in electronic devices and appliances, from microdisplays and small handheld mobile phones to medium-sized notebook and desktop computers and large-panel LCD TVs. After decades of development, LCD technology is capable of giving excellent image performance at a relatively low cost. Compared with other display technologies, a unique characteristic of LCDs in terms of maintaining long-term competitiveness is the vigorous technical progress being made in almost every key element, including the LC material, TFT, LC cell structure, color filters, compensation films (including polarizers), backlight source, backlight films, driving electronics and algorithms, etc. In the foreseeable future, LCDs will continue to maintain their dominance in the display market.

Presently, three types of LCD have been developed to suit different applications: (i) transmissive, (ii) reflective, and (iii) transflective LCDs. In a transmissive LCD, a backlight is usually embedded as the light source to illuminate the LCD panel. A transmissive LCD typically exhibits high

Transflective Liquid Crystal Displays Zhibing Ge and Shin-Tson Wu

brightness (300–500 cd/m^2), high contrast ratio (>1000 : 1), and good color saturation. With its high image quality, transmissive LCD is the most adopted display technology and its performance is being improved steadily. For example, with film compensation and a multi-domain structure, a contrast ratio over 50 : 1 can now be easily obtained omnidirectionally in a wide-view LCD TV. Utilizing new backlight sources, like RGB light emitting diodes (LEDs), the color gamut can reach over 110% of NTSC to show pretty rich and vivid colors. With advanced low-viscosity LC materials and fast LC modes, a refresh rate of over 120 Hz (i.e., 240 Hz or even 480 Hz) has been achieved. Together with backlight local dimming, the dynamic image qualities, including dynamic contrast ratio and motion picture response time, have also been continuously enhanced which, in turn, leads to a significant energy saving. Therefore, for mobile displays, the high image quality of a transmissive LCD is advantageous, but some of its features mean it is still imperfect for mobile applications. First, transmissive LCDs rely on backlight white LEDs to illuminate the image. The associated power consumption is relatively high, resulting in a short battery life. Second, for some outdoor situations such as under strong sunlight, the surface luminance provided by a backlight cannot compete with the sunlight, leading to a washed out image and poor outdoor readability. Although increasing backlight intensity to elevate surface brightness above the ambient light intensity could improve the readability, the power consumption would also be dramatically increased. A solution for reaching good sunlight readability of a transmissive LCD is to embed an ambient light intensity sensor into a pure transmissive LCD that can dynamically or smartly adjust the brightness of the backlight to meet different ambient conditions. But this approach can only really target short usage times given the power consumption needed. For example, most transmissive mobile displays have a surface luminance at about 200 to 300 cd/m^2. To compete with regular outdoor sunlight (direct sunlight > 100 000 lux), huge backlight power is required to increase surface luminance to over 500 cd/m^2, even with anti-reflection coatings on the display front surface.

Another type of display is the reflective LCD, which embeds a metal reflector behind the LC cell, such as a mixed twisted nematic cell [1, 2] or cholesteric cell [2, 3], and uses external light to illuminate the displayed image. A reflective LCD has low power consumption and good sunlight readability. On the other hand, since a reflective LCD relies on external light to display the image, it exhibits poor readability in a low ambient light environment. Besides, the imperfect removal of surface reflection degrades its contrast ratio and color performance. Its low reflectivity (in most cases using circular polarizers), low contrast ratio (a typical value is ~5 : 1, while a

diffusive white paper has a contrast ratio of $\sim$15 : 1) and low color saturation give viewers a different image experience from what would be seen on a transmissive LCD. Therefore, reflective LCDs are usually employed for low-end applications, such as devices that only require outdoor daytime viewing. Nevertheless, their low power consumption and sunlight readability are superior to transmissive displays, making reflective LCDs useful in portable devices where battery life is critical.

As a direct consequence, transflective LCDs have been designed to combine both transmissive and reflective functions into one display [4, 5]. In dark or low ambient light conditions, the backlight is turned on and the image is mainly displayed in the transmissive mode, exhibiting excellent image quality with high contrast ratio and good color saturation. In a bright ambient light situation such as under strong sunlight, the reflective mode mainly functions to display images and the backlight may either be turned on to assist the image display or turned off to save power. According to different application requirements, the ratio of transmissive to reflective regions can be varied. For instance, for a portable audio player that requires longer battery life, a larger reflective region can be adopted. But for a video cell phone where a vivid image is very important, the transmissive region can be made larger. Driven by the increasing demands of the mobile electronics market, high brightness, wide viewing angles, vivid color, fast response, outdoor readability, and low cost are all now required for small mobile displays. Research into transflective LCDs is being undertaken to meet such requirements.

In this book we will focus on the mainstream TFT-addressed wide-view transflective LCDs for mobile applications. First, the fundamental device elements including polarizers, liquid crystal alignment, relevant compensation films, reflectors, and backlight films that comprise a portable LCD device and their associated principles are briefly introduced. This is followed by the introduction of related modeling methods of LCD directors and optics which serve as the basis for transflective LCD characterization and optimization. More details on developing good light efficiency and wide viewing angle transflective LCDs are then discussed in terms of both TFT LC cell design and compensation films. Advanced topics related to applications like touch panels and fast response time for video mobile displays will also be addressed. Finally, Chapter 6 re-addresses the unique and irreplaceable role of transflective LCDs in the mobile display market and discusses the possible directions in which they could be developed to enhance competitiveness.

Figure 1.1 depicts the device structure of an active matrix-driven transmissive LCD based on amorphous silicon (a-Si) thin-film-transistor (TFT) technology. An LCD is a non-emissive display, i.e., it does not emit light by

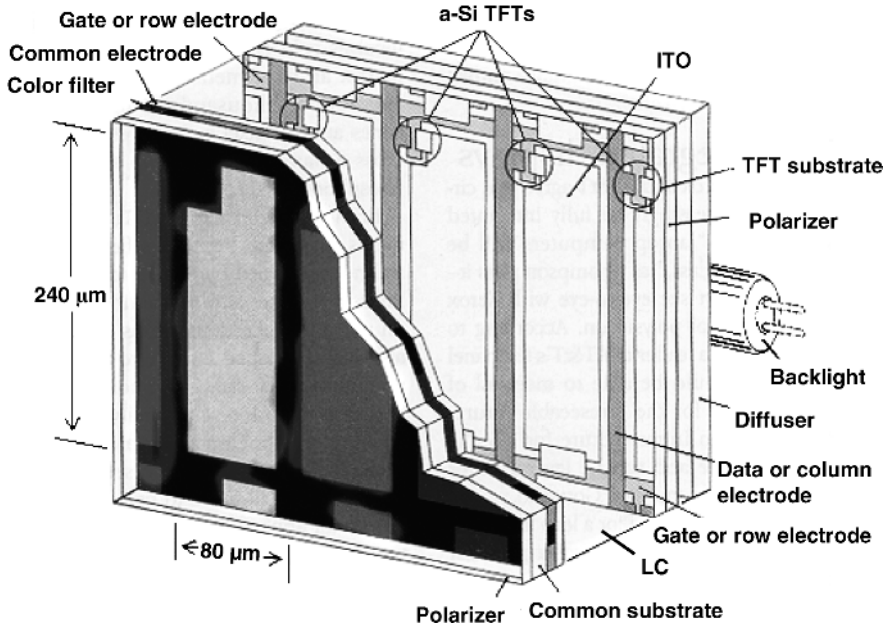

Figure 1.1 Device structure of one pixel (with RGB sub-pixels) of a transmissive TFT LCD

itself; instead, it utilizes a backlight and the LC cell sandwiched between two sheets of stretched dichroic polarizers functions as a light valve. A diffuser close to the backlight is used to homogenize the backlight intensity in order to avoid hot spots. Prism films, such as 3M´s brightness-enhancement-film (BEF) [6] are stacked to confine the incident Lambertian backlight into a central cone to $\pm 40^{\circ}$ for enhancing axial display brightness. On the rear substrate (the TFT-array substrate), a TFT-array is formed to provide an independent switch for each pixel. Color filters are fabricated on the front substrate (namely the color-filter-array substrate) and aligned with the rear TFT pixels. In each time frame, signals (short high-voltage pulses) from the gate lines turn on the TFTs in a scanning sequence, and the voltages from the data lines are applied thereafter to drive each individual LC pixel to the targeted gray level. Under such a spatial RGB-sub-pixel configuration, different colors are achieved by combining the separate colors from RGB sub-pixels at assigned gray levels, and the eyes average the overall optical response from them. For large-panel TV applications, the typical sub-pixel size is about $80\,\mu m \times 240\,\mu m$. The sub-pixel size is reduced to about $50\,\mu m$ $150\,\mu m$ in small cell phone panels. In practice, the effective aperture for light

transmission is much smaller than the sub-pixel area. The aperture ratio, defined as the effective region for transmission over the total region of each pixel, is usually less than 80%. Several factors cause a low aperture ratio. For TFTs, the active channel is sensitive to visible light, requiring a light shielding layer to cover that region. To avoid light leakage and color mixing from adjacent sub-pixels, black matrix (BM) is also formed at the boundaries between sub-pixels. The metal or alloy gate and data lines and the storage capacitor, made of opaque material, lead to a further reduction in the aperture ratio. Even for the area that is transparent to light, the light transmission cannot always reach 100% owing to the LC alignment there. In some LC modes such as the multi-domain vertical alignment (MVA) LCD [7–9], non-desired LC reorientations such as disclination lines also lower the effective light output.

For the LC cell, both inner surfaces are coated with a thin ($\sim$80 nm) polyimide layer to provide initial alignment of LC molecules that will adjust the ordered LC reorientation when a voltage is applied. Presently, major LCD technologies like twisted nematic (TN) [10], in-plane switching (IPS) [11, 12], fringe field switching (FFS) [13], and pi-cell or optically-compensated-bend (OCB) cells [14, 15] require a surface rubbing alignment, and technologies based on the VA mode, such as MVA [7–9], and patterned vertical alignment (PVA) [16] can yield initial vertical alignment without rubbing for high contrast. The LC cell gap is usually controlled at about 4.0 μm for a transmissive LCD, and the phase change of the LC layer between a fully bright state and a dark state is about half a wavelength. The electro-optical performance of the display in terms of light efficiency, response time, and viewing angle is related to the LC material, alignment, and cell structure.

For a direct-view reflective LCD, the cross-sectional view is depicted in Figure 1.2. This device utilizes external ambient light to display images, where incident light is reflected by the rear reflector and traverses the LC cell twice. The front linear polarizer and the retardation film (such as a quarter-wave plate) form a crossed-polarizer configuration for incident light. The aperture ratio of a reflective LCD is much higher than that of a transmissive one, since the TFT, and storage capacitor can be buried under the metal reflector. The cell gap of the LC layer is typically about 2 μm and the phase change between the bright state and the dark state is about quarter of a wavelength. Here, the color filter layer is formed on the front substrate in the figure, but alternatively it could be formed on the rear glass substrate. To avoid specular reflection and widen the viewing angle, a bumpy reflector surface is usually required and asymmetrical reflection is preferred, i.e., the incident angle and exit angle of the rays are designed to be different. Thus, strong surface specular reflection, which is considered noise, will not

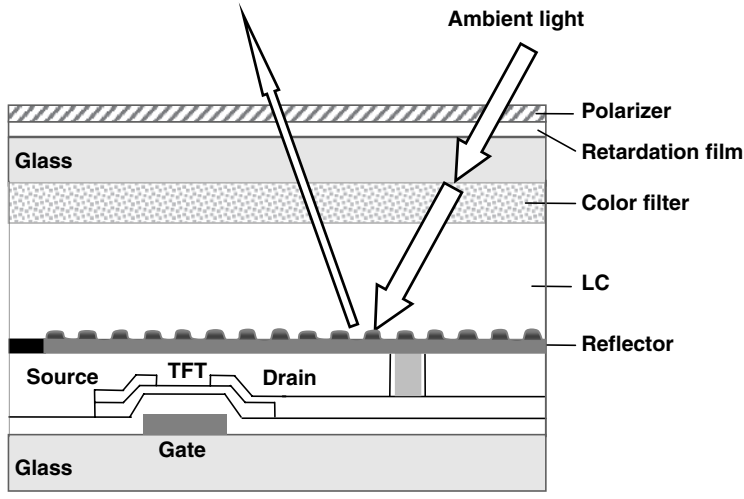

Figure 1.2 Device structure of one sub-pixel of a reflective TFT LCD

overlap with the useful signal coming out of the LC cell. Compared with a transmissive LCD, the contrast ratio, viewing angle, and color saturation of a reflective LCD are inferior, resulting from many factors such as non-negligible surface reflection, complex optical films for circular polarizer configuration, and uncolored openings on the color filters for high reflectivity. Research efforts are being made to improve the image quality of reflective LCDs, e.g., by designing new anti-reflection films and high-reflectivity reflectors.

1.2 Polarizers

1.2.1 Linear Polarizers

As discussed above, optical performance of an LCD relies on each optical element, such as the LC cell, compensation film, and polarizer. For transmissive LCDs, linear polarizers partially determine the contrast ratio and hue balance (the spectral distribution of light output from the polarizers) of the display. For reflective LCDs, circular polarizers, comprising both a linear polarizer and a quarter-wave plate, are usually employed where viewing angle and dark-state spectral light leakage are important. Below, we will briefly introduce different polarizers employed in LCDs and their associated mechanisms. Typically, linear polarizers for LCDs are made from

polyvinyl-alcohol (PVA) films with iodine compounds using the wet-dyeing method [17]. After the PVA is stretched, dichroic species, such as I_3^- and I_5^- complexes, are aligned along the stretching direction, thus light polarized along this stretch direction will be strongly absorbed, while light polarized perpendicular to this direction will be transmitted. The degree of polarization and transmittance of PVA-stretched polarizers is highly dependent on the dichroism and the amount of dichroic species. In other words, one can control these parameters to adjust the transmittance and hue balance of the polarizers, which is very important for displays, especially for LCD TVs.

Figure 1.3 shows the optical transmittance from two identical linear polarizers set parallel or perpendicular to each other. For the parallel setup, the output transmittance in the blue region is much weaker than that at longer wavelengths. Here, the absorption of light is proportional to $\exp\left(-\frac{2\pi}{\lambda}dn'\right)$, where λ is the wavelength, d is the thickness of the medium, and n' is the imaginary part of the refractive index of the polarizer along the transmission or absorption axis. In a typical polarizer, the transmission axis n' (of the order of 10^{-5}) decreases as wavelength increases. Blue light (with a smaller λ value) experiences a larger $\exp\left(-\frac{2\pi}{\lambda}dn'\right)$ value and in turn a stronger absorption than red light through two parallel polarizers. As a result, a weaker output of blue light in the bright state causes the so-called *blue decoloration phenomenon*, making the display at full bright state appear a little yellowish. On the other hand, light leakage from these two crossed linear polarizers is inherently well suppressed over most of the visible range, although there is still evident light

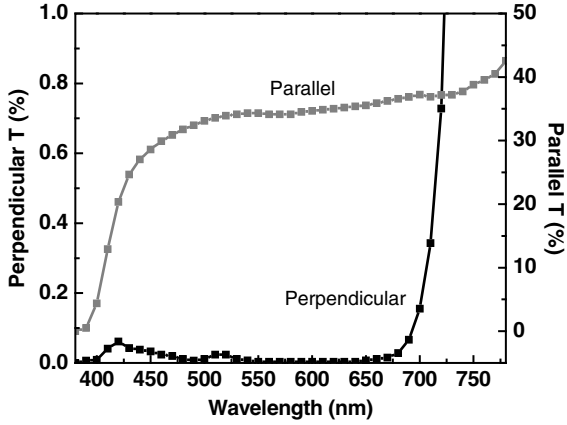

Figure 1.3 Wavelength-dependent transmittance of two linear polarizers at parallel (open) and perpendicular (closed) positions

leakage in the blue and red regions, as shown in the figure, causing decoloration of both bluish and reddish colors in the dark state. To eliminate or reduce decoloration for a better color balance, material engineering is applied. Each dichroic species has unique absorption peaks at different wavelengths and we can control the I_3^- and I_5^- complexes to increase the absorption in the blue region to suppress bluish decoloration in the dark state. Sometimes compensation films, including optimized TAC films, are also helpful in reducing the color shift of the dark state [17, 18]. For the bright state color balance, in addition to optimizing the material properties, we can adjust the transmittance of each color via backlight or LC cell engineering (controlling the output transmittance of each sub-pixel) to compensate for the weak blue color, achieving a balanced white point.

1.2.2 Circular Polarizers

The polarizer configuration for reflective or transflective displays, however, is more complicated than that of a transmissive display. Previously, for reflective LCDs used in low-end products like wrist watches, two crossed linear polarizers were employed to sandwich the LC layer and a metal reflector or transflector was formed behind the rear polarizer [5, 19]. Since the total thickness of the rear polarizer (including protective layers) and the LC substrate is much larger than the LC cell gap and the pixel size, parallax occurs, which creates a shadow image when the display is viewed at oblique angles, thus degrading the image quality of the display [5]. Of course, if a high-performance, in-cell polarizer could be fabricated, this issue would be solved. But the formation of an in-cell polarizer is very complicated and they are not easy to mass produce. Thus, for reflective LCDs, the metal reflector should be placed adjacent to the LC layer to avoid this parallax. Under such a configuration, to form an effective crossed polarizer reflective mode structure, a circular polarizer needs to be placed in front of the LC cell. The rear polarizer is eliminated. A typical circular polarizer consists of a linear polarizer and a uniaxial quarter-wave plate, as shown in Figure 1.4. The quarter-wave plate has its optical axis aligned at 45° away from the transmission axis of the front linear polarizer. Hence, linearly polarized light from the front linear polarizer will first be converted to right-handed circular polarization (RCP) by the quarter-wave plate. The RCP light is then reflected by the metal reflector, and its polarization becomes left-handed circular polarization (LCP) as the propagation direction is reversed. Note the light maintains its absolute rotation in the lab *x*-*y*-*z* coordinate sense, as shown in Figure 1.4. The LCP light is then converted by the quarter-wave plate into

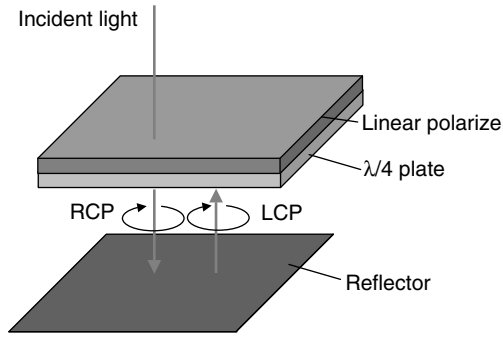

Figure 1.4 Configuration of a circular polarizer using a linear polarizer and a quarter-wave plate

linearly polarized light perpendicular to the front linear polarizer transmission axis, and is blocked. Using circular polarizers in a transmissive LCD based on the MVA mode can also greatly increase the light efficiency owing to the removal of azimuthal angle dependence of LC directors [20, 21].

The configuration shown in Figure 1.4 is simple but has the following issues: (i) high spectral light leakage, and (ii) high off-axis light leakage. The quarter-wave plate has quarter-wave retardation only at a single wavelength (e.g. 550 nm), and it is incapable of covering the whole visible spectrum. Figure 1.5 illustrates wavelength-dependent light leakage at normal and at

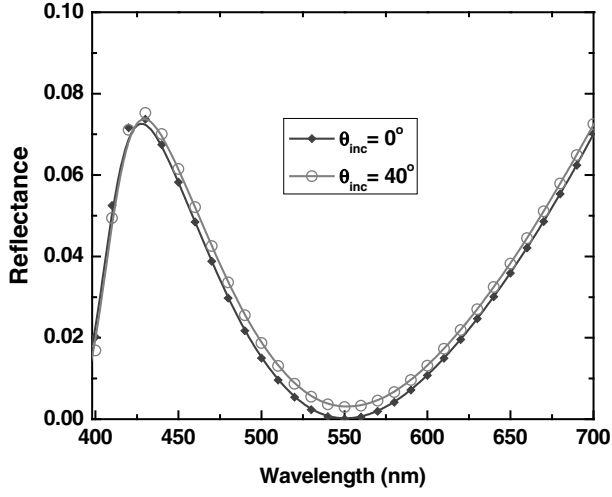

Figure 1.5 Spectral light leakage from a monochromatic circular polarizer

40° incidence. Relatively high light leakage occurs at wavelengths other than the central wavelength of 550 nm, and it increases at oblique incidence. In addition to the imperfect absorption of the linear polarizer used (as shown in Figure 1.3), another important reason for the high spectral light leakage of the configuration in Figure 1.4 is the wavelength dispersion of the quarter-wave plate. Here the birefringence (Δn) of a polymeric retardation film can be roughly estimated as $\Delta n \propto A + \frac{B}{\lambda^2 - \lambda_0^2}$ [17, 22], where A and B are constants, and λ_0 is the absorption edge wavelength and is usually in the ultraviolet range. As the wavelength λ increases, Δn will decrease and $d\Delta n/\lambda$ in turn decreases farther away from the desired value.

From the above analysis, the first method to suppress spectral light leakage is to design new quarter-wave plates with a reverse birefringence (Δn) dispersion by stacking plates with different Δn dispersions, i.e., $d\Delta n/\lambda$ remains roughly a constant throughout the visible range [17, 18]. For example, a quarter-wave plate of reverse dispersion can be manufactured based on subtraction by stacked half-wave and quarter-wave plates with different wavelength dispersions, while their optical axes are set perpendicular to each other. A rough illustration of this method is shown in Figure 1.6. This approach is simple, but the overall dispersion obtained from two real polymeric materials might still be far from an ideal reverse dispersion curve, where $d\Delta n/\lambda$ would remain constant throughout the visible range.

A second method is to stack several retardation plates with different optical axis alignment to self-compensate the wavelength dispersion. Unlike the first

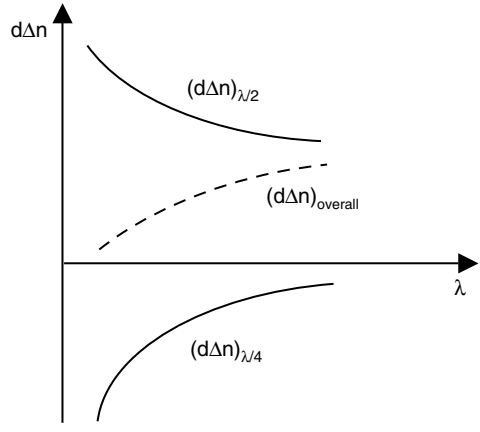

Figure 1.6 Reversed dispersion achieved by stacking a half-wave plate and a quarter-wave plate with different dispersion relations

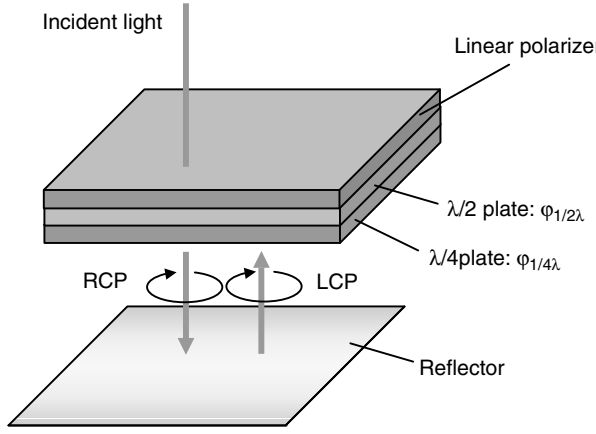

Figure 1.7 Broadband circular polarizer achieved by stacking a linear polarizer, a half-wave plate, and a quarter-wave plate

method, here the retardation plates can have either the same or different dispersion. Using this second approach, it is easier to achieve good dispersion compensation and this method is now widely adopted in practical circular polarizer designs. As shown in Figure 1.7, the broadband circular polarizer consists of a linear polarizer (transmission axis at 0°), a monochromatic half-wave plate (optical axis at $\varphi_{1/2\lambda}$), and a monochromatic quarter-wave plate (optical axis at $\varphi_{1/4\lambda}$) [21]. Here the relation of these angles can be demonstrated from the polarization change trace on the Poincaré sphere [23, 24]. Figure 1.8(a) illustrates the polarization trace of the incident light at a designated wavelength on the Poincaré sphere. Assuming the transmission axis of the linear polarizer is at point **T** on the Poincaré sphere, the optical axis of the first half-wave plate is at point **H**, with $\angle TOH = 2\varphi_{1/2\lambda}$, and the optical axis of the quarter-wave plate is at point **Q**, with $\angle TOQ = 2\varphi_{1/4\lambda}$ (here the relative angle of the optical axis represented on the Poincaré sphere is twice the absolute value in *x*-*y*-*z* coordinates). The linearly polarized light from the front linear polarizer is first rotated from point **T** along **OH** by half a circle when traversing the first half-wave plate; thus, its polarization goes to point **C** at $\angle TOC = 4\varphi_{1/2\lambda}$. The next quarter-wave plate converts the linear polarization from point **C** to RCP on the north pole, i.e., the $\angle QOC$ should be 90°. Hence, $2\varphi_{1/4\lambda} - 4\varphi_{1/2\lambda} = 90°$ is required for this configuration to function as a circular polarizer. Moreover, to obtain broad bandwidth operation, the value of $\varphi_{1/2\lambda}$ is also very important. Figure 1.8(b) roughly depicts the polarization change of different wavelengths (R: 650 nm, G: 550 nm, and B: 450 nm, where each retardation film thickness is designed only for 550 nm). The retardation value $d\Delta n/\lambda$ is inadequate for red

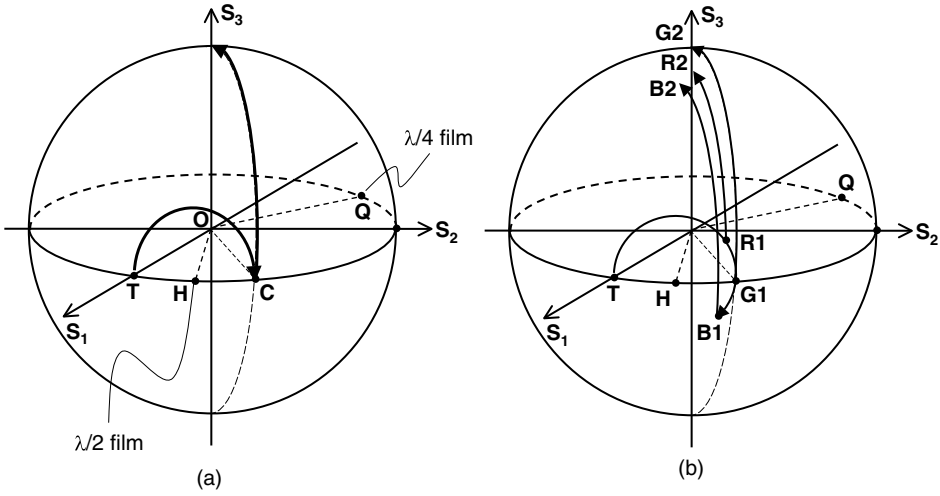

Figure 1.8 Polarization traces on the Poincaré sphere from the broadband circular polarizer for (a) green light (550 nm) and (b) R, G, and B light at normal incidence

light, but too high for blue light. As a result, after the first half-wave plate, the polarizations for red, green, and blue light locate at points **R1**, **G1**, and **B1**, respectively. The location of red light at **R1** is closest to the north pole, thus the subsequent inadequate phase from the quarter-wave plate can still convert light close to circular polarization at the north pole. Similar compensation also occurs for blue light. From this analysis, in addition to the above alignment relation, $\varphi_{1/2\lambda}$ is also very important for such self-compensation of the wavelength. An optimized angle for $\varphi_{1/2\lambda}$ is about 15°, thus $\varphi_{1/4\lambda}$ is about 75° [21]. To achieve broadband operation, the polarization traces from the half-wave plate and the quarter-wave plate should stay in the same upper or lower hemisphere.

The spectral light leakage from the configuration in Figure 1.7 can be greatly suppressed at normal incidence. However, this design still exhibits off-axis light leakage, and with more retardation films, its off-axis performance could be even worse than the above-mentioned monochromatic circular polarizer at the center wavelength, as shown in Figure 1.9. For mobile reflective or transflective LCDs using circular polarizers, a wide viewing angle is also critically important. Especially for transflective LCDs, the transmissive subpixel will be sandwiched between circular polarizers, and high off-axis light leakage is not acceptable. Additional compensation schemes are needed to achieve both a wide viewing angle and broadband operation in circular polarizers, which will be discussed in detail in Chapter 3.

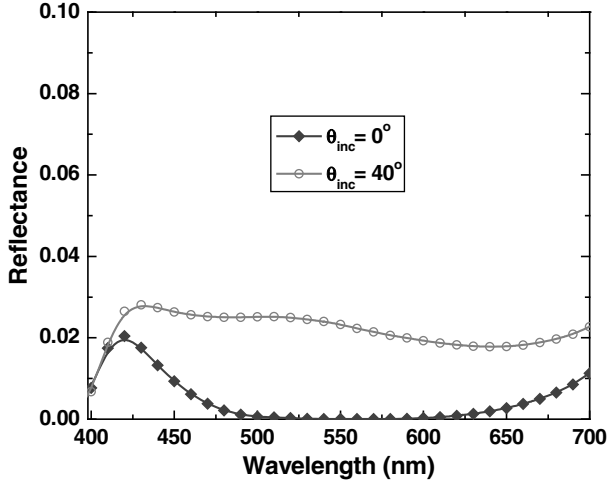

Figure 1.9 Simulated light leakage from the broad-band circular polarizer at normal and oblique angles

1.3 LC Alignment

To be used in display devices, LC mixtures need to be confined and aligned with specific pre-orientation between two substrates made from, for example, glass or plastic. Three commonly used alignment methods are mechanically rubbed polyimide (PI), ion beam etched PI, and evaporated SiO_x [25]. With its simple fabrication process, rubbed PI is the most popular alignment method. Inorganic SiO_x based alignment is mainly adopted in projection displays owing to its robustness and ability to withstand high-intensity illumination.

The initial surface alignment of LCs determines the electro-optical properties of the LC device. For initial molecular distribution, various LC cell alignment technologies, including homogeneous alignment, twisted nematic alignment, vertical alignment, pi-cell alignment, and hybrid alignment, have been developed [4]. Below, we will briefly address the main characteristics and applications of several mainstream LC alignment technologies.

1.3.1 Twisted Nematic (TN) Mode

Twisted nematic alignment [10] is the most commonly used liquid crystal technology for small and medium-sized LCD panels. The basic configuration of a TN cell with LC director profile at the bright (voltage-off) and dark

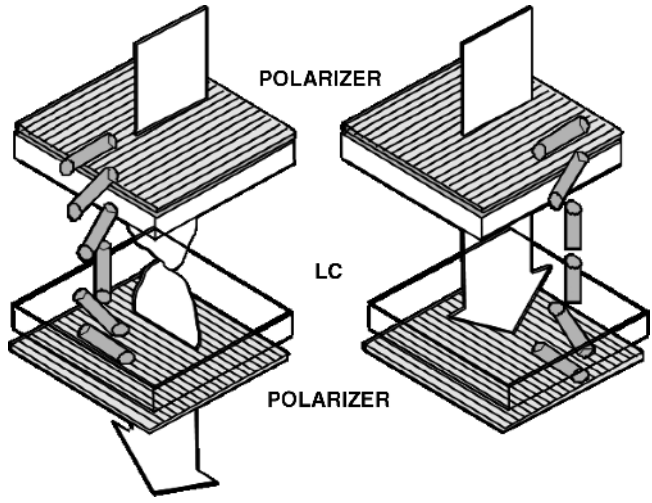

Figure 1.10 Configuration of a TN cell in the voltage-off (left) and voltage-on (right) states

(voltage-on) state is shown in Figure 1.10. The front and rear LC surfaces are rubbed at an angle difference of 90°, thus the LC optical axis gradually twists by 90° from rear to front when no voltage is applied. When a relatively high voltage is applied, the vertical electric field between the rear and front substrates makes the LC directors tilt vertically in the bulk region, as shown in Figure 1.11, where ϕ and θ stand for the azimuthal and polar angles, respectively. When a relatively high voltage is applied (such as $V = 5V_{\text{th}}$, where V_{th} is the threshold voltage), the whole LC cell seems to consist of three parts: a thick vertical-alignment-like cell in the central bulk region with most directors tilted vertically, and two crossed thin hybrid-alignment-like cells near the surfaces. The continuously twisted LC director distribution in the voltage-off state and tri-layered structure in the voltage-on state lead to several unique electro-optical characteristics of 90° TN cells between two crossed linear polarizers.

The normalized transmittance ($T_{\perp}$) of a TN cell with twist angle ϕ and cell gap d under crossed linear polarizers can be expressed as:

$$T_{\perp} = \cos^2 X + \left(\frac{\Gamma}{2X}\cos 2\beta\right)^2 \sin^2 X, \tag{1.1}$$

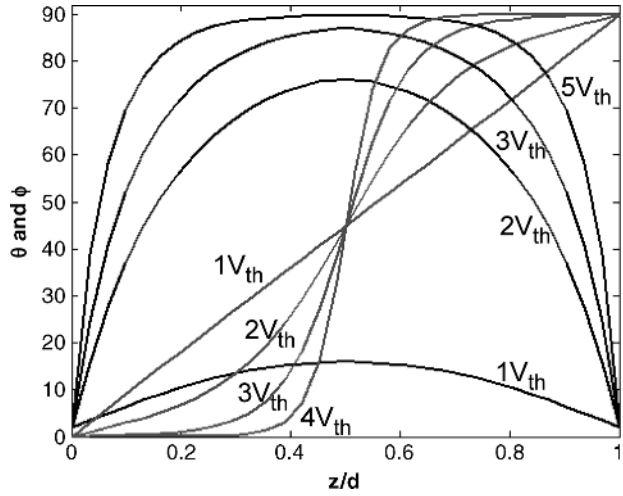

Figure 1.11 LC director profile of a TN cell at different voltages. Dark lines represent tilt angles and gray lines twist angles

where $X = \sqrt{\phi^2 + (\Gamma/2)^2}$, $\Gamma = 2\pi d\Delta n/\lambda$, and β is the angle between the polarization axis and the front LC director. As we can see, when $\cos^2 X = 1$ ($X = m\pi$ and m is an integer), the transmittance will be independent of β as the second term in the equation vanishes. By setting $X = m\pi$ and given $\Gamma = 2\pi d\Delta n/\lambda$, we can obtain the so-called Gooch–Tarry condition for a 90° TN cell ($\phi = 90°$):

$$\frac{d\Delta n}{\lambda} = \sqrt{m^2 - \frac{1}{4}}. \tag{1.2}$$

Typically, the first minimum condition with $m = 1$ and $d\Delta n/\lambda = \sqrt{3}/2$ is adopted for TN cells.

Figure 1.12 plots the voltage-dependent transmittance for three primary wavelengths of displays at R = 650, G = 550, and B = 450 nm. Since human eyes are most sensitive to green light, we optimize the transmittance of the TN cell at $\lambda = 550$ nm. In a 90° TN cell with β at 0° or LC rubbing direction parallel to the polarizer transmission axis, wavelength dispersion is relatively small (compared with a homogeneous or vertical alignment cell). In addition, the TN cell also has a relatively easy fabrication process and good light efficiency, making it the preferred technology in most LCD devices that do not require a wide viewing angle.

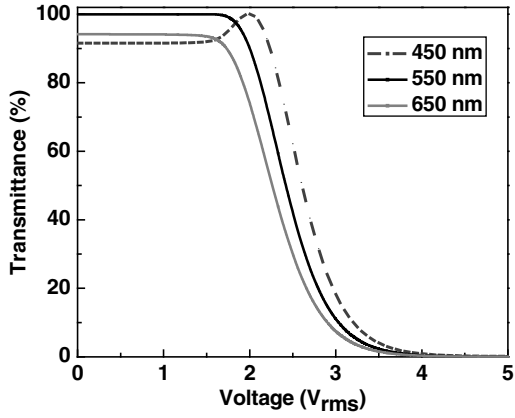

Figure 1.12 Voltage-dependent transmittance of a normally white 90° TN cell with $d\Delta n = 480\,\text{nm}$

The drawbacks of a TN cell are its narrow viewing angle and gray level inversion when used without compensation film, resulting from its inherent LC director distribution in the dark state. Referring to Figure 1.11, the tri-layered structure in the dark state has two hybrid-alignment-like thin layers near the boundaries, and a vertical-alignment-like cell in the bulk. At normal incidence, the two thin boundary layers are crossed to each to cancel the phase retardation, leading to a good dark state. But at off-normal incidence, these three different layers all cause phase retardation, leading to a narrow viewing angle. The butterfly-shaped iso-contrast plot for the TN cell at $\lambda = 550\,\text{nm}$ with protective tri-acetyl cellulose (TAC) films is shown in Figure 1.13, where the contrast ratio drops quickly away from normal incidence. A relatively narrow viewing angle limits the application of the TN cell to small to medium-sized displays.

The narrow viewing angle results from several factors, e.g., optical anisotropy of LCs from the tri-layered structure in the dark state, off-axis light leakage from two crossed linear polarizers (or effective polarizer angle deviation), and light scattering in the color filters. To increase the viewing angle of a TN cell, compensation film is needed; this should be able to compensate for the tri-layered structure and the effective polarizer angle deviation. One commonly employed wide-view (WV) film is the discotic film developed by Fujifilm Company [26, 27]. Details of the compensation scheme are plotted in Figure 1.14, where a discotic material (triphenylene derivatives) is coated on an alignment layer on a TAC substrate near each polarizer´s inner surface. The discotic material is in a hybrid alignment configuration with the

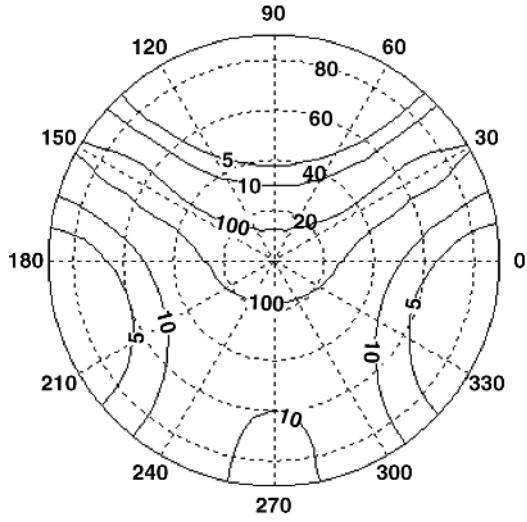

Figure 1.13 Iso-contrast plot of a 90° TN cell at $\lambda = 550$ nm with protective TAC films

following important features: (i) it has π-electrons spread in a disk-like shape, which gives rise to a high birefringence (much larger than a typical compensation film), and (ii) it exhibits a discotic nematic phase at a lower temperature than that at which the TAC starts to deform, enabling a uniform formation of the film on the TAC substrate [26]. The discotic material adjacent

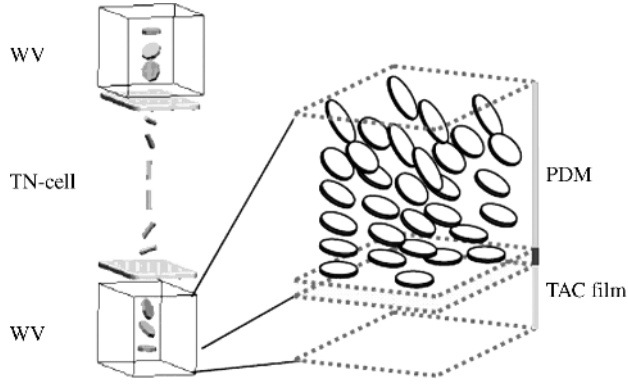

Figure 1.14 Wide-view discotic film for TN LCD (courtesy of K. Takeuchi *et al.* (27), Reproduced by permission of SID)

to the alignment layer on the TAC substrate has a high degree of randomness and its molecules tend to align with the molecular plane almost parallel to the alignment layer, with a few degrees of pre-tilt in the alignment layer rubbing direction. On the other hand, in the vicinity of the air surface, the discotic molecules tend to align with the molecular plane almost perpendicular to the air surface. Thus, the controllable alignment near the two surfaces forms a hybrid alignment structure of the film. After UV curing, the discotic material is polymerized to become a polymerized discotic material (PDM) like a film, which also exhibits a fixed structure over a large temperature range.

The WV film can be laminated to polarizing film by a roll-to-roll process. Optically, to compensate for the TN mode, the WV film is usually employed in an O-mode TN LCD with the polarizer transmission axis perpendicular to the adjacent LC surface rubbing direction. The PDM film has its azimuthal direction aligned perpendicular to the nearby polarizer transmission axis. Here the TAC film is a biaxial film (i.e., $n_z < n_y <$ or $\cong n_x$), exhibiting a small phase retardation. However, this TAC film (along with the discotic PDM film) is also critical in phase compensation. Figure 1.15 shows the iso-contrast plot of a TN LCD by incorporating the WV film with both PDM and TAC films. Compared with the previous result, the viewing angle is significantly

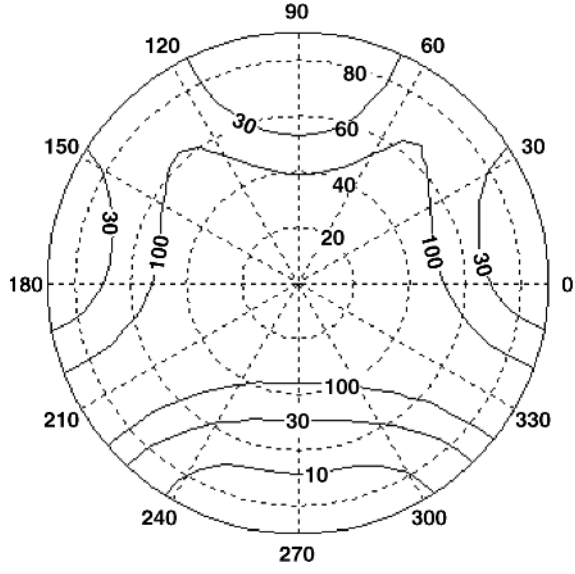

Figure 1.15 Iso-contrast plot of a 90° TN cell at $\lambda = 550$ nm with both protective TAC films and WV films

increased and becomes more symmetrical. However, such viewing angle performance is still inadequate for applications like large-panel LCD TVs, for which advanced LCD modes like in-plane switching (IPS) and multi-domain vertical alignment (MVA) are more favored.

1.3.2 Homogeneous Alignment Mode

In a homogeneous alignment cell, the alignment layers are initially anti-parallel rubbed with a certain pre-tilt angle for the boundary LCs. When a relatively high voltage is applied between rear and front plane electrodes, vertical electric fields cause the LC molecules to tilt up. Figure 1.16 shows both the off-state and on-state LC director profiles and light polarization changes in a homogeneous cell between two crossed linear polarizers. The homogeneous alignment mode belongs to the ECB (electrically controlled birefringence) family, where a pure phase retardation effect dominates in modulating the polarization of the incident light. For a phase retarder (with thickness d, birefringence Δn, and wavelength λ) inserted between two crossed linear polarizers, if the optical axis is aligned at an angle of ϕ with respect to the absorption axis of the rear linear polarizer, the output light intensity can be written as $I = I_o \sin^2 2\phi \cdot \sin^2(\delta/2)$, where δ is the phase retardation value at $2\pi d\Delta n/\lambda$, and I_o is the maximum output light intensity from two such parallel linear polarizers. To obtain maximum transmittance, ϕ should be equal to 45° and $\delta = (2m + 1)\pi$, where m is an integer. In most cases, $m = 1$ in order to shorten the response time.

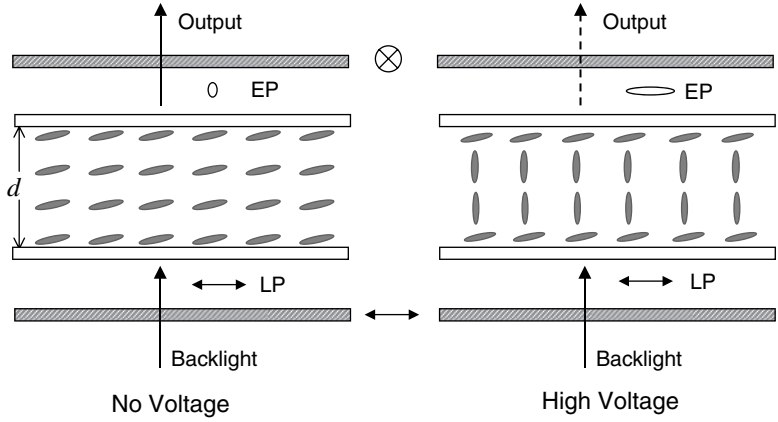

Figure 1.16 LC director distributions and changes of light polarization in a homogeneous cell in the voltage-off and voltage-on states

A homogeneous LCD with the LC rubbing direction at 45° to the transmission axis of the linear polarizer is a normally white display. Under a relatively high voltage, positive dielectric anisotropic ($+\Delta\varepsilon$) LCs will be driven to become vertically aligned to the substrate, to have a reduced effective δ and in turn lower the output transmittance. However, due to the strong surface anchoring force, surface LC molecules will still be aligned at their initial pre-tilt angles. Thus, a small residual wavelength retardation will exist even if a relatively high voltage is applied. In order to eliminate such surface residual retardation to achieve a good dark state, compensation films are needed. In applications using transflective LCDs, an ECB-based dual-cell-gap device is one of the mainstream technologies, where the surface phase residual retardation can be cancelled by quarter-wave plates in the adjoining circular polarizers, as will be discussed in Chapter 3. Generally, a homogeneous base LCD exhibits a narrow viewing angle, owing to the surface LC distribution in the dark state. In addition, with a single-domain structure, gray level inversion is also quite severe. To widen the viewing angle, complicated compensation films such as discotic films are also required.

1.3.3 In-plane Switching (IPS) Mode

In a TN or homogeneous cell, the LC molecules are perturbed by the longitudinal electric fields between the two substrates. Thus, different LC profiles and phase retardations are observed when viewed from the left, right, upper, or lower directions, yielding an asymmetrical and narrow viewing angle. In contrast, an IPS cell uses interdigitated electrodes formed on the same rear glass substrate to generate transverse electric fields to reorient the LC molecules horizontally, leading to a more symmetrical viewing angle. IPS technology was first proposed in the 1970s [11] and later implemented in TFT LCDs in the 1990s [12]. Figure 1.17 plots the IPS cell structure with corresponding LC director profile and equal potential lines. Here, the electrode width w is about 4 μm and the spacing distance l is about 8 μm. When the spacing distance is larger than the cell gap, strong horizontal electric fields mainly exist between the common electrode (black) and the pixel electrode (gray). With proper surface alignment, LC molecules are rotated by the horizontal fields to induce phase retardation of incident light. The optimized angle between the surface rubbing direction and the longitudinal direction of the electrode is determined by a compromise between light efficiency, operating voltage, and response time. Typically the optimized angle is about 10° when using a $+\Delta\varepsilon$ LC material and about 80° when using a $-\Delta\varepsilon$ one. On the other hand, as electric fields are mostly vertical in the regions in front of the

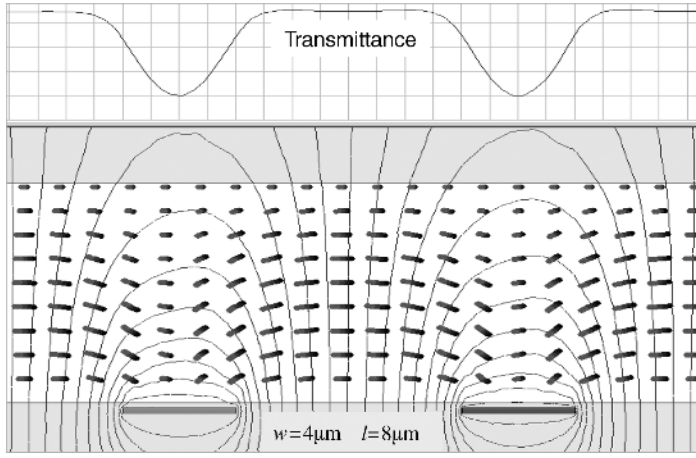

Figure 1.17 IPS cell configuration with director profile, equi-potential lines, and transmittance curve

electrode strips, LC molecules with a $+\Delta\varepsilon$ would tilt up most there, causing a loss of phase retardation and low transmittance for the incident light, as shown in the plot. Overall, the light efficiency in an IPS cell using a $+\Delta\varepsilon$ LC material is only about 75% of that of a TN LCD. Using a $-\Delta\varepsilon$ LC material in an IPS structure enhances the value to over 80%, but the driving voltage is increased because negative LC mixtures usually exhibit a smaller $|\Delta\varepsilon|$, i.e., a higher threshold voltage.

To improve light efficiency while maintaining the horizontal movement of LC molecules, fringe-field switching (FFS) mode was developed [13]. An FFS cell using a $-\Delta\varepsilon$ LC material is shown in Figure 1.18 with LC director profile and equi-potential lines included. Here, the common electrode is planar in shape and pixel electrodes are in strips. Typically the pixel electrode has a width $w \sim 3\,\mu m$ and a gap $g \sim 5\,\mu m$. Here, although the electrode gap g is larger than the cell gap (about 4 μm), the actual horizontal distance between a pixel electrode edge and the common electrode is zero. As a result, stronger fringe fields with both horizontal and vertical field components will be generated to perturb the LC molecules. Moreover, we can observe different dynamic mechanisms between an IPS cell and an FFS cell. In an IPS cell, strong horizontal electric fields are formed between the pixel and common electrodes to rotate the LC molecules parallel to the substrate, while the LCs in front of the electrode strips mainly tilt up. But in an FFS cell, fringe fields with much stronger horizontal fields are only formed near the electrode edges (equi-potential lines there are denser) and decrease towards the centers of electrode

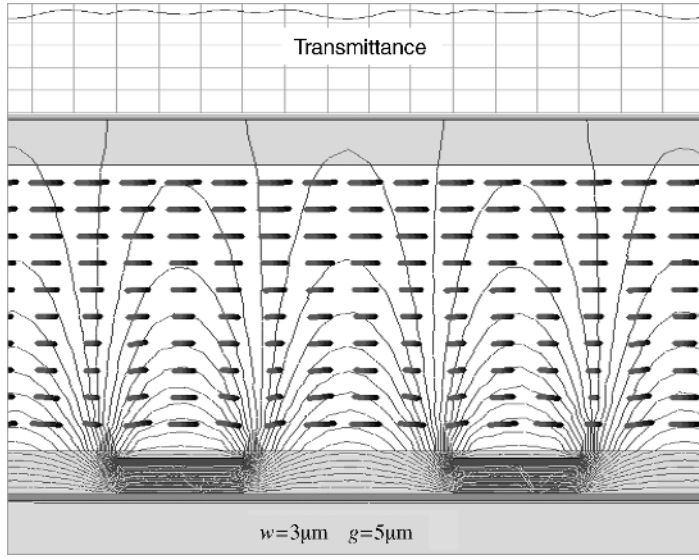

Figure 1.18 FFS cell configuration with equal potential lines and transmittance curve. The voltage difference between the front pixel electrode strips and the rear planar common electrode is 4.5 V_{rms}

strips or gaps. The strong horizontal fields near the edges rotate the LCs there in-plane first. Owing to the small dimensions and stronger fields, this perturbation near the edges in turn propagates horizontally in both directions to cause the reorientation of LCs near the centers of the electrodes or gaps where the field lines are vertical. Because of this unique process, the transmission of an FFS cell can be greatly enhanced to reach over 95% of that of a TN cell by using a $-\Delta\varepsilon$ LC material and over 85% by using a $+\Delta\varepsilon$ one. Usually, a $+\Delta\varepsilon$ LC material is preferable in an FFS LCD, since it has a larger $\Delta\varepsilon$ value and a lower viscosity, thus its operating voltage and response time can be reduced. In addition to the high transmission efficiency, other characteristics of an FFS cell make it more popular: (i) the capacitance between the front pixel electrodes and the rear common electrode can contribute to the storage capacitance of the pixel, which further improves the aperture ratio of the display, and (ii) because of the horizontal reorientation of LC molecules, an FFS cell exhibits weak color dispersion, which is an advantage compared to TN or VA cells. The second one is also true for IPS cells. More details of the FFS mode will be discussed in Chapter 4.

A detailed investigation of the mechanisms by which we can obtain high transmittance in IPS or FFS cells is of interest. To study the origins of high light

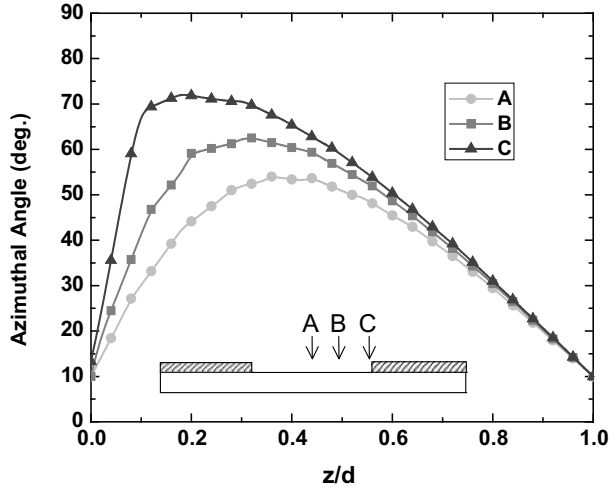

Figure 1.19 LC twist profiles at different positions in an FFS cell

efficiency, we plot, in Figure 1.19, the LC azimuthal angle distributions at different cell positions: gap center at position **A**, intermediate position **B** between gap center and electrode edge, and electrode edge at position **C**. The LC twist angle is largest at position **C** where horizontal fields are strongest, and decreases as the position approaches the center of the electrode gap. More importantly, the on-state LC profile is like two TN cells with opposite twist senses and the peak twist angle plays a critical role in the output light efficiency.

The polarization trace of light traversing the LC cells from these three different positions in an FFS cell at normal incidence is plotted in the S_1–S_2 plane (S_1 and S_2 are Stokes parameters), as shown in Figure 1.20. (For an introduction to light polarization in LCDs represented by Stokes parameters on the Poincaré sphere, the reader should refer to Chapter 3.) Light with linear polarization parallel to the rear polarizer transmission axis is defined as $S_1 = +1$ at point $\mathrm{T}_{\mathbf{rear}}$, which is the starting point for the light incident towards LC from positions **A**, **B**, and **C**. Thus, the front linear polarizer transmission axis perpendicular to the rear polarizer can be designated at point $\mathrm{T}_{\mathbf{front}}$ by $S_1 = -1$. With a peak twist angle larger than 45° across a very thin cell gap at position **C**, the light polarization there quickly moves to the lower half-plane with $S_2 < 0$. And then the front TN structure rotates the polarization in a different curvature, adjusting the final polarization close to the point $\mathrm{T}_{\mathbf{front}}$. With a smaller peak twist angle ($< 45°$ away from the initial angle) at position

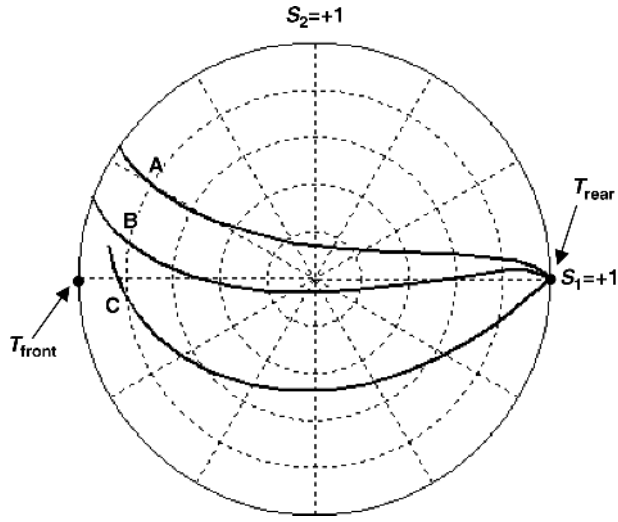

Figure 1.20 Polarization traces of light traversing the FFS cell from different positions at normal incidence

A, the light polarization trace is mainly above the S_1 axis in the upper half-plane with $S_2 > 0$. The inadequate maximum twist angle in both rear and front half TN cells makes the final polarization depart away from the point T_{front}, outputting a smaller light transmittance there. Therefore, peak twist angle is important for obtaining high transmittance, and a two-TN-cell structure would make the transmittance less sensitive to wavelength dispersion.

Figure 1.21 shows the VT curves of the FFS structure for three primary display wavelengths at R = 650, G = 550, and B = 450 nm. The driving voltage of this FFS cell using a $-\Delta\varepsilon$ LC material is about 4.5 V_{rms}, and the cell is optimized at a wavelength of 550 nm. An inset plot is also included to compare the VT curves at the three wavelengths, where each curve is normalized to its own maximum value. The R, G, and B curves overlap perfectly with each other, originating from the two-TN-cell configuration of the on-state LC director profile in the FFS cell, as analyzed earlier.

Another important feature of IPS and FFS cells is their inherent wide viewing angle. The iso-contrast plot for an uncompensated FFS cell using a $-\Delta\varepsilon$ LC material is plotted in Figure 1.22. A contrast ratio of 10:1 can be achieved to about 70° in all directions. If a $+\Delta\varepsilon$ LC material is used, the rotation of the LC directors will be influenced by the vertical electric field components, resulting in a lower transmittance ($\sim$ 85%) and a narrower viewing angle (contrast ratio 10:1 to about 60°). But a $+\Delta\varepsilon$ LC usually has a

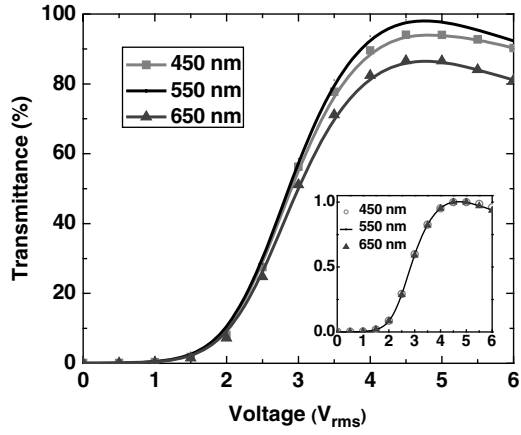

Figure 1.21 VT curves of R, G, and B light for a 4 μm normally black FFS cell. The inset plot shows the normalized curves; the three curves overlap perfectly

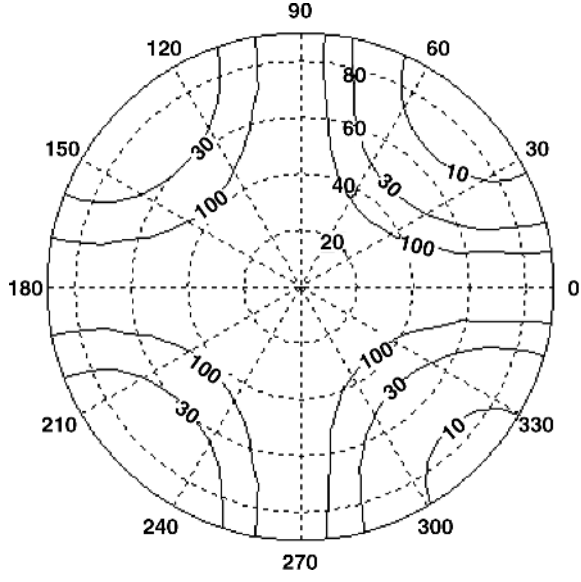

Figure 1.22 Iso-contrast plot of an FFS cell at $\lambda = 550$ nm without compensation films

larger $\Delta\varepsilon$ value and smaller rotation viscosity, leading to a lower driving voltage and faster response time. The wide viewing angle and weak color dispersion make FFS extremely attractive for small-panel mobile displays.

1.3.4 Vertical Alignment (VA) Mode

The homeotropic cell, also called a vertical alignment (VA) cell, is another mainstream LCD technology, owing to its super high contrast ratio. In a VA cell, the LC directors are almost perpendicular to the surface alignment layers, thus the axial light leakage between two crossed linear polarizers is much lower than in a homogeneous cell, TN cell, or even an IPS cell. Figure 1.23 shows the LC director profiles in the voltage-off and voltage-on states of a single-domain VA cell. In the voltage-off state, the incident light maintains its polarization when traversing the LC cell, and is then blocked by the front linear polarizer independent of the incidence wavelength, leading to a good dark state for all wavelengths. In a relatively high voltage state, the bulk LC directors tilt down, causing phase retardation for the incident beam. Similar to the homogeneous cell, for a single-domain VA cell, the optical axes of the surface LC molecules are controlled at $\pm 45^\circ$ from the polarizer transmission axis for maximum transmission. The output transmission intensity I also satisfies $I = I_o \sin^2 2\phi \cdot \sin^2(\delta/2)$ and the associated polarization change of incident light is purely dependent on the phase retardation of the LC cell, which is similar to a pure uniaxial wave plate. Consequently, the output

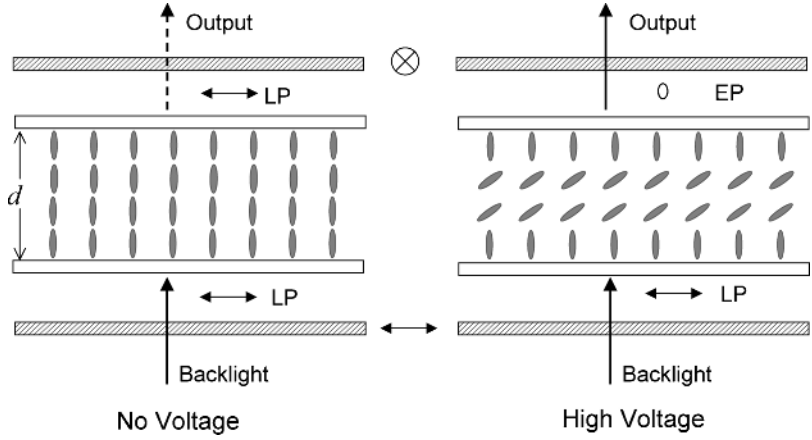

Figure 1.23 LC director distributions and light polarization changes in a homeotropic cell (or VA cell) in voltage-off and voltage-on states (LP: linear polarization; EP: elliptical polarization)

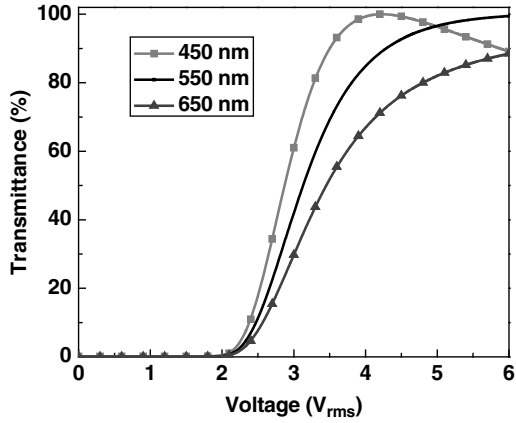

Figure 1.24 VT curves of R, G, and B wavelengths for a 4 μm VA cell

transmission is strongly wavelength dependent, which can be clearly seen from Figure 1.24.

A single-domain VA cell exhibits a narrow viewing angle and severe gray level inversion. To increase the viewing angle, both film compensation and a multi-domain structure are needed. Fujitsu [7–9] developed the first multi-domain vertical alignment (MVA) technology by introducing protrusions on both glass substrates, as shown in Figure 1.25(a). With small pre-tilt angles on the protrusion surfaces, the LC directors can be adjusted to tilt in different directions, forming two domains. A four-domain structure can be achieved with zigzag electrodes and protrusions. This early design required a complicated fabrication process to make the protrusions on both substrates, and

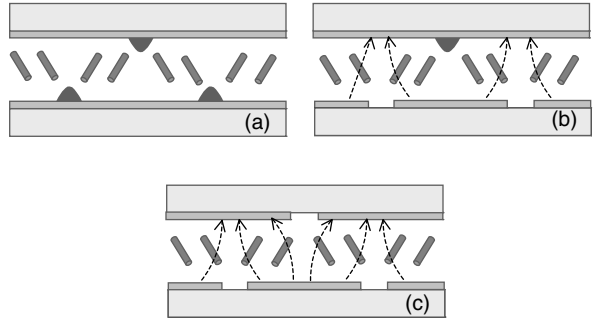

Figure 1.25 Structures of MVA cells using (a) protrusions only (by Fujitsu), (b) both protrusions and slits (by Fujitsu), and (c) slits only (PVA by Samsung)

exhibited low contrast due to the LC pre-tilt near the protrusions. To improve the contrast, opaque materials were employed to make protrusions, but the aperture ratio was consequently reduced by locally blocking light transmission. To solve these issues, Fujitsu [8] later proposed an improved MVA version, as shown in Figure 1.25(b), where the rear protrusions were replaced by electrode slits. This structure can effectively guide LC directors to form multi-domains by adjusting effects from both the pre-tilt angles on the front protrusions and the fringing fields near the rear electrode slits. Slits can be utilized on both substrates to further improve the contrast of the VA cell. This concept was first outlined in the work of Alan Lien and colleagues [28–30] and has been developed by Samsung, as shown in Figure 1.25(c), as the patterned vertical alignment (PVA) mode [16]. However, without the small pre-tilt on the protrusions, the dynamic response of the PVA cell is slower than the MVA cell using protrusions. To decrease the response time, special driving schemes to give the LCs an initial pre-tilt by means of a small bias voltage are helpful [31].

Owing to their high contrast and wide viewing angle (with compensation films), MVA and PVA LCDs are the technologies most widely employed for TV and monitor applications. For small-panel transflective LCDs, besides the wide viewing angle, MVA cells have the following features that are quite attractive: (i) the optical configurations for combining transmissive and reflective modes are relatively simple, requiring only circular polarizers, and (ii) it is possible to compensate for the optical path difference between transmissive and reflective modes by applying different electric fields to each mode in a single cell gap configuration. But VA mode also has certain drawbacks such as low response time, low light efficiency, and severe surface pooling. Surface pooling is an optical effect that occurs when the panel surface is touched or pressed, making it look like water pooling. It is caused by the distortion of LC directors inside the LC cell and a long restoration time is needed when negative dielectric anisotropic LC materials are used. Fortunately, new technologies such as novel electrode design and polymer-sustained surface alignment technology [32, 33] greatly help to solve these issues. Detailed discussion of MVA in transflective LCD designs will be presented in Chapter 4.

1.3.5 Hybrid Aligned Nematic (HAN) Mode

Hybrid aligned nematic (HAN) mode is a special liquid crystal alignment that combines different surface alignment on each of the two surfaces: a homogeneous alignment on one substrate and a vertical alignment on the other [34].

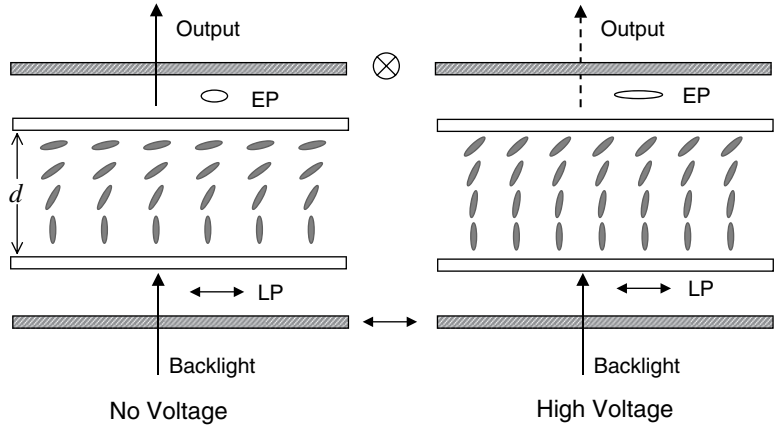

Figure 1.26 LC director distributions and changes of light polarization in a HAN cell in the voltage-off and voltage-on states

The LC director distributions of a HAN cell in the voltage-off and voltage-on states can be seen in Figure 1.26. Compared with a pure homogeneous cell or a VA cell with the same cell gap, the effective phase retardation of the HAN cell is reduced to about half of the $d\Delta n$ value. In addition, when a relatively high voltage is applied, the LC molecules near the homogeneous alignment surface remain parallel to the substrate, yielding residual phase retardation and light leakage.

This unique hybrid alignment structure enables several special display applications: (i) it is a useful alignment for the reflective region to achieve single-cell-gap operation in a transflective LCD, when the transmissive region uses a normal VA or homogeneous alignment, and (ii) it forms special optical compensation films to compensate for the dark state of the TN cell, homogeneous cell, or pi-cell that has a HAN profile near the substrate in the dark state [35, 36]. Detailed application examples will be discussed later.

1.3.6 Pi-cell or Optically Compensated Bend (OCB) Alignment Mode

The pi-cell, where the two substrate surfaces are treated with parallel rubbing, was first reported in 1984 [14, 15]. Typically the pi-cell is pre-controlled at an initial bend state, as shown in Figure 1.27(a). Without any treatment such as a bias voltage, the pi-cell usually stabilizes at a splay state. The transition from a splay state to a bend state takes quite a long time, sometimes even up to minutes for large panels. Thus, for fast switching purposes, it is preferable to

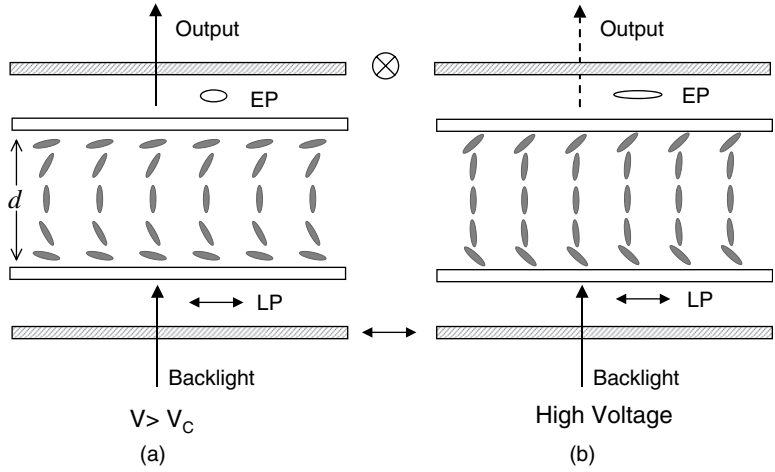

Figure 1.27 LC director distributions and light polarization changes in a pi-cell at (a) the initial state and (b) the voltage-on state

switch the cell between the bend state in Figure 1.27(a) and a high tilt state in Figure 1.27(b). In practice, to maintain a stable initial bend state, the LC free energy in the bend profile needs to be lower than that in a splay distribution. Approaches including a bias voltage above a critical voltage or high surface pre-tilt angles [37] can be utilized to stabilize the bend state.

The fast response time of the pi-cell, resulting from the flow effect and half-cell switching [14], is quite attractive. Figure 1.28(a) depicts the flow in a homogeneous cell with anti-parallel rubbing. After the electric field is switched off, the surface anchoring forces function to relax the LC molecules back to their initial state, causing horizontal flows in the cell. As indicated by the small arrows showing the flow directions, the LC directors around the center face a torque that rotates them opposite to the general tendency. This

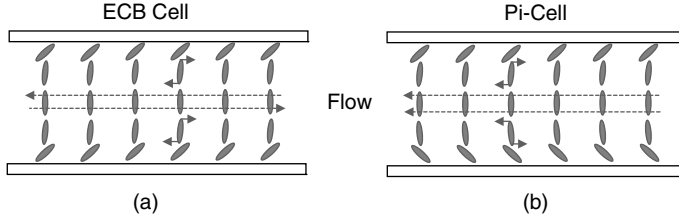

Figure 1.28 Comparisons of flows between (a) a homogeneous cell and (b) a pi-cell during the relaxation stage

causes 'back-flow' that slows down the switching-off time. Optically, the back-flow causes an 'optical bounce' during the relaxation process in the time-dependent transmittance curve. A pi-cell does not exhibit such a back-flow phenomenon, as shown in Figure 1.28(b). The flow directions originating from the front and rear surfaces have the same direction for the central LC directors. Thus, LCs near the bulk center behave in a 'stabilized' way and the switching-off time is much faster.

Similar to the homogeneous cell described above, in the voltage-on (or dark) state, residual phase retardation exists due to the surface LC molecular orientation. Thus, to obtain a common dark state for different incident wavelengths, compensation films are needed to cancel such residual phase retardation. In addition, in the dark state, the surface LC distribution is like that of a HAN cell, and a discotic film is also suitable for phase compensation of a pi-cell to suppress off-axis light leakage [38]. The fast response time and symmetrical viewing angle of the pi-cell make it quite attractive for mobile displays involving video applications.

1.4 Compensation Films

To obtain a high contrast ratio and wavelength-independent dark state, normally black modes like IPS (or FFS) and MVA (or PVA) are preferable to the normally white types using TN or homogeneous cells. In IPS (or FFS) and MVA (or PVA) cells, the LC layer in the voltage-off state does not modulate the polarization of normally incident light. But at oblique incidence, light leakage still occurs, especially in the bisector directions (the directions with an incident azimuthal angle $\pm 45^\circ$ away from the absorption axis of the polarizers). Such light leakage results from two sources: (i) the deviation of effective polarizer angle, and (ii) the off-axis phase retardation of the LC layer itself.

1.4.1 Deviation of Effective Polarizer Angle

Figure 1.29 shows a general representation of the effective angle between two auxiliary axes viewed on an oblique incident wave plane. In the x–y plane, for axis **OM** at azimuthal angle ϕ_1 and axis **ON** at angle ϕ_2 with respect to the reference x-axis, their angular difference is $\phi_2 - \phi_1$ when viewed from the normal z-axis. But this angular difference varies as the viewing direction changes from the z-axis to an oblique direction along **OK** in the plot. Based on the dot product of vectors, the effective angle $\angle$MKN between the projected lines **KM** and **KN** viewed on the wave plane **MKN** can be calculated and expressed as [23]:

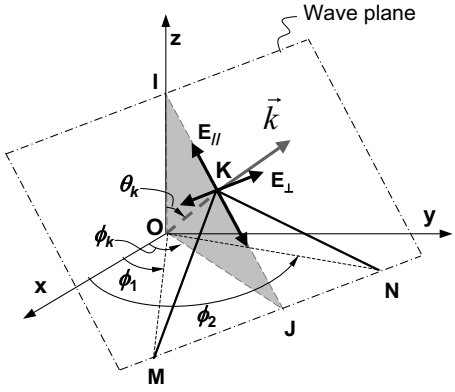

Figure 1.29 A representation of the effective angle viewed on an oblique incident wave plane between two auxiliary axes

$$\varphi = \cos^{-1}\left[\frac{\cos(\phi_2-\phi_1)-\sin^2\theta_k\cos(\phi_2-\phi_k)\cos(\phi_1-\phi_k)}{\sqrt{1-\sin^2\theta_k\cos^2(\phi_2-\phi_k)}\sqrt{1-\sin^2\theta_k\cos^2(\phi_1-\phi_k)}}\right], \tag{1.3}$$

where θ_k and ϕ_k are the polar angle and azimuthal angle in the medium of the wave vector $\vec{k}$ respectively. For light incident at a polar angle of θ_0 from the air on to the medium, the polar angle may be obtained as $\theta_k = \sin^{-1}(\sin\theta_0/n_p)$ in the medium with n_p ($\sim$1.5) defined as the real part of the average refractive index of the medium.

For the special case of two crossed linear polarizers with $\phi_2 - \phi_1 = 90°$, the above equation can be written in another form in terms of $\phi_1 - \phi_k$ as:

$$\begin{aligned}\varphi &= \cos^{-1}\left[\frac{1/2\cdot\sin^2\theta_k\sin 2(\phi_1-\phi_k)}{\sqrt{1-\sin^2\theta_k+(1/2\cdot\sin^2\theta_k\sin 2(\phi_1-\phi_k))^2}}\right] \\ &= \cos^{-1}\left[\frac{sign[\sin 2(\phi_1-\phi_k)]}{\sqrt{(1-\sin^2\theta_k)/(1/2\cdot\sin^2\theta_k\sin 2(\phi_1-\phi_k))^2+1}}\right].\end{aligned} \tag{1.4}$$

Therefore, at any polar angle of θ_0, when $\phi_1 - \phi_k = \pm 45°$, the absolute value of $(\varphi - 90°)$ reaches the maximum at $\pi/2-\cos^{-1}\left(\frac{\sin^2\theta_0/n_p^2}{2-\sin^2\theta_0/n_p^2}\right)$, i.e., the effective angle of two polarizers deviates the most from the initial crossed configuration

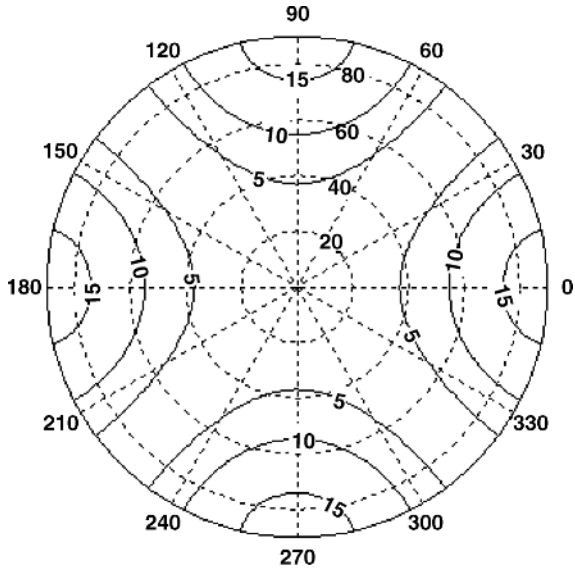

Figure 1.30 Angular-dependent deviations of the effective polarizer angle from 90°

at 90°. Thus, the incident azimuthal directions at ±45° from the polarizer transmission axis are defined as the bisector directions, where light leakage is most severe. Figure 1.30 plots the deviation of the effective polarizer angle from 90° ($\varphi - 90°$ in absolute value) with respect to different viewing azimuthal angle values ($\phi_1 - \phi_k$), which agrees well with the above analysis. For two crossed linear polarizers, normally incident light could be well absorbed, as the light passing the rear linear polarizer has a polarization direction parallel to the absorption axis of the front one. However, at off-axis incidence (such as at a polar angle of 70° along the bisector direction), the two polarizers are no longer perpendicular to each other and the light passing the rear linear polarizer will have a polarization direction away from the front linear polarizer absorption axis, leading to light leakage. To suppress the light leakage resulting from this deviation of the effective polarizer angle, compensation films can be used to adjust the light coming out of the rear linear polarizer to coincide with the front linear absorption axis. Detailed analysis of the compensation method based on the Poincaré sphere will be discussed in Chapter 3.

1.4.2 Phase Retardation from Uniaxial Medium

Besides the deviation of effective polarizer angle, the phase retardation of the LC cell itself also causes a change in polarization and leads to imperfect light

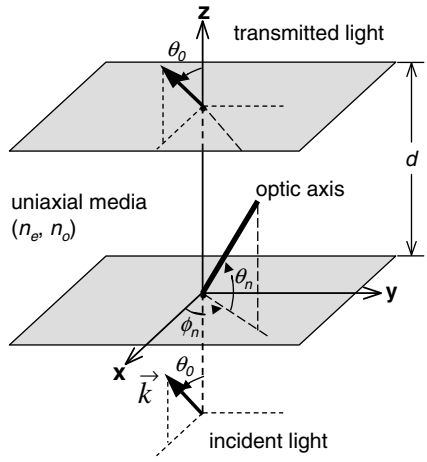

Figure 1.31 Schematic view of light propagation through a uniaxial medium with the incident wave vector in the *x–z* plane

absorption. The LC layer can be treated as a uniaxial layer with extraordinary and ordinary refractive indices n_e and n_o. When light propagates through a uniaxial medium, generally two eigenwaves with different phase velocities are excited, thus phase retardation occurs, which changes the light polarization. Figure 1.31 depicts light propagation through a uniaxial medium. Without losing generality, the optical alignment of incident light can be set into the x–z plane with a propagation vector $\vec{k}$ of (sin θ_0, 0, cos θ_0), and a uniaxial layer with extraordinary and ordinary refractive indices at n_e and n_o, optical axis at (cos ϕ_n, sin θ_n), and a thickness of d.

The phase retardation of a uniaxial medium at oblique incidence can be expressed by the phase difference between the extraordinary wave, which has a wave number k_{ez} along the z-axis, and the ordinary wave, which has k_{oz} as $\Gamma = (k_{ez} - k_{oz})d$ [39–41]. A solution of the Maxwell equation for wave propagation through a uniaxial medium can lead to expressions for k_{ez} and k_{oz} as follows [39–41]:

$$k_{ez} = k_0 \left[-\frac{\varepsilon_{xz}}{\varepsilon_{zz}}\frac{k_x}{k_0} + \frac{n_o n_e}{\varepsilon_{zz}} \sqrt{\varepsilon_{zz} - \left(1 - \frac{n_e^2 - n_o^2}{n_e^2}\cos^2\theta_n \sin^2\phi_n\right)\left(\frac{k_x}{k_0}\right)} \right]$$
$$= \frac{2\pi}{\lambda} \left[\frac{n_e n_o}{\varepsilon_{zz}} \sqrt{\varepsilon_{zz} - \left(1 - \frac{n_e^2 - n_o^2}{n_e^2}\cos^2\theta_n \sin^2\phi_n\right)\sin^2\theta_0} - \frac{\varepsilon_{xz}}{\varepsilon_{zz}}\sin\theta_0 \right], \quad (1.5)$$

and

$$k_{oz} = k_0 \left[\sqrt{n_o^2 - \left(\frac{k_x}{k_0}\right)^2} \right] = \frac{2\pi}{\lambda} \left[\sqrt{n_o^2 - \sin^2\theta_0} \right]. \tag{1.6}$$

where λ is the incident wavelength, ε_{zz} and ε_{xz} are the tensor components of the uniaxial medium, $\varepsilon_{zz} = n_o^2 + (n_e^2 - n_o^2)\sin^2\theta_n$ and $\varepsilon_{xz} = \varepsilon_{zx} = (n_e^2 - n_o^2)$ $\sin\theta_n \cos\theta_n \cos\phi_n$. Detailed derivation of these equations will be presented in Chapter 2. With these known variables, the phase retardation $\Gamma = (k_{ez} - k_{oz})d$ of the light propagating through the uniaxial layer can be determined.

For a homogeneous LC cell (if the small surface pre-tilt angle is neglected), the LC layer behaves optically like a positive uniaxial A-film; for a vertical alignment LC cell, the LC layer behaves optically like a positive uniaxial C-film. With $\theta_n = 0^\circ$ and 90° for the A-film and C-film respectively, the phase retardations can be expressed as:

$$\Gamma_a = \frac{2\pi}{\lambda} d \left[n_e \sqrt{1 - \frac{\sin^2\theta_0 \sin^2\phi_n}{n_e^2} - \frac{\sin^2\theta_0 \cos^2\phi_n}{n_o^2}} - n_o \sqrt{1 - \frac{\sin^2\theta_0}{n_o^2}} \right], \tag{1.7}$$

and

$$\Gamma_c = \frac{2\pi}{\lambda} d \left[n_o \sqrt{1 - \frac{\sin^2\theta_0}{n_e^2}} - n_o \sqrt{1 - \frac{\sin^2\theta_0}{n_o^2}} \right]. \tag{1.8}$$

1.4.3 Uniaxial and Biaxial Films

From the above analysis, the off-axis phase retardation of the LC cell could change the incident light polarization, causing light leakage. To minimize off-axis light leakage, compensation films are needed to operate on light leaving the LC layer, so that when it reaches the second linear polarizer it is linearly polarized parallel to the absorption axis of that polarizer. Figure 1.32 shows an optical retardation film with refractive indices n_x, n_y, and n_z and of thickness d. Optical compensation films can be divided into different categories based on different standards. For example, based on the relation between its refractive indices n_x, n_y, and n_z, they can be classified as uniaxial films with only one optical axis or biaxial films with two optical axes. Uniaxial films can further be classified into A-films and C-films, where an A-film has its optical axis parallel to the film surface ($n_e = n_x \neq n_o = n_y = n_z$) and a C-film has the optical

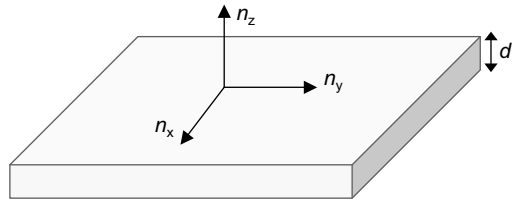

Figure 1.32 Typical parameters of a phase compensation film

axis perpendicular to the film surface ($n_e = n_z \neq n_o = n_x = n_y$). Furthermore, both A-films and C-films can be divided into positive or negative ones, depending on the relative value between the extraordinary refractive index n_e and the ordinary refractive index n_o: a positive film has $n_e > n_o$ and a negative one has $n_e < n_o$. On the other hand, if $n_x \neq n_y \neq n_z$, the retardation film has two optical axes, and is called a biaxial film. In addition to directly using n_x, n_y, n_z and its thickness d, a retardation film is also widely characterized in other ways by:

1. N_z factor, where $N_z = \frac{(n_x - n_z)}{(n_x - n_y)}$;
2. in-plane phase retardation $R_0 = (n_x - n_y)d$;
3. in-thickness phase retardation $R_{th} = [(n_x + n_y)/2 - n_z] \cdot d$;
4. average refractive index.

These parameters represent different optical interpretations of the phase retardation [42]. These uniform films all have their optical axes aligned in the same direction, either parallel or perpendicular to the film surface. In addition, there are some special films that have their optical axes inclined or non-uniformly distributed. For example, the above-mentioned Fuji film has negative discotic molecules in a hybrid alignment, an NH film has regular nematic LC molecules in a hybrid alignment, and an O-plate has its nematic LC molecules uniformly inclined by a certain tilt angle [43]. These films are mainly used to compensate LCDs having irregular LC director profiles in the dark state, such as TN cells, homogeneous cells, and pi-cells.

Optical films can be formed by different methods such as coating liquid crystalline materials or stretching polymer films [17, 44, 45]. For example, an A-film can be formed by coating and polymerizing discotic LC molecules in a sideward alignment for negative birefringence, like coins standing on edge, or by coating and polymerizing nematic rod-like LC molecules in a homogeneous alignment for the positive type, or by stretching polymer materials to align polymer chains with the stretching direction. Whether this creates

positive or negative birefringence depends on the side polymer chain structure and its alignment to the backbone. A C-film can be formed by coating and polymerizing nematic rod-like LC molecules in a homeotropic alignment for positive birefringence or short-pitched cholesteric nematic LC molecules for negative birefringence. Fuji films or NH films can be formed by coating discotic material or nematic material on a special alignment layer whilst controlling the formation conditions such as temperature. Biaxial films can also be formed by using the polymer-stretching method by stretching in two directions or by the coating method. Presently, fabrication methods for most uniaxial films are well developed, except for negative A-films, for which it is still difficult to obtain large birefringence and good quality in mass production. The fabrication technology for biaxial films has advanced quickly, and now these films are widely used for IPS and MVA LCDs, for which only uniaxial films dominated previously. However, it is still difficult to make biaxial films with certain pre-designed refractive indices and thickness, but sometimes special biaxial film parameters can be realized by stacking two or more different attainable biaxial films to produce the required optical performance.

1.5 Reflectors

The reflector and transflector are important components of transflective LCDs, since dual functions (transmissive and reflective) exist in the device simultaneously. An ideal reflector or transflector is required to reflect the incident ambient light towards the viewer in a confined cone with high reflectivity but also with a certain amount of diffusion to widen the viewing angle; and it should also avoid overlap between the major reflected beams and the front surface specular directional ambient light reflection. Surface treatment is critical to meet these requirements. In addition, the position of a reflector or transflector is also critical in order to avoid parallax. To better understand these requirements, the two concepts of parallax and ambient contrast ratio will be introduced. Then, different types of reflectors and transflectors and their application to mobile LCDs will be addressed.

1.5.1 Parallax and Ambient Contrast Ratio

Parallax occurs when a reflective LCD is viewed at an oblique angle [5], when the directly viewed image of a pixel and its image viewed in the reflector are separated by a distance comparable to or greater than the pixel size. It causes cross talk between pixels and loss of contrast. Figure 1.33 demonstrates an example of parallax in a reflective LCD when the polarizer and reflector are

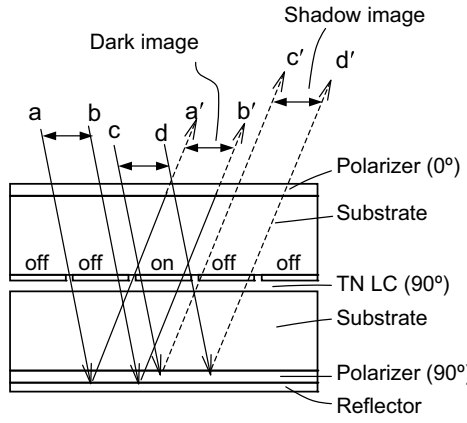

Figure 1.33 Schematic illustration of the parallax phenomenon in a reflective LCD

laminated on the outer side of the rear thick substrate. This sample is a normally white 90° TN reflective LCD that is widely used in low-end displays like electronic watches or calculators. At normal incidence, when no voltage is applied (off-state), the incident ambient light is transmitted by the LC cell with a 90° polarization rotation to pass through the rear linear polarizer and is then reflected, with an opposite 90° rotation, to pass back through the front linear polarizer to produce a bright image. When a relatively high voltage is applied (on-state), the incident light passing the LC cell sees a negligible rotation and is then blocked by the rear linear polarizer, leading to a dark image. When looking at the on-pixel at an off-axis direction, as shown in Figure 1.33, the viewer sees two types of 'dark' image. The first one, designated **a′–b′**, originates from the incident light source **a–b**, where the light first traverses the left off-pixel (having a 90° rotation) and further through the rear linear polarizer on to the reflector, and is then reflected back to transmit the on-pixel and finally becomes absorbed by the front linear polarizer. The second dark image, designated **c′–d′**, originates from the incident light source **c–d**, which passes through the on-pixel (maintaining its polarization) and is finally blocked by the rear linear polarizer before reflection, and **c′–d′** is its image to the viewer. Here, dark image **a′–b′** is caused by the front linear polarizer and image **c′–d′** results from the rear linear polarizer. The thick rear substrate and linear polarizer make the incident and exit light pass different pixels, creating cross talk between pixels. Images **a′–b′** and **c′–d′** shift from each other; this phenomenon is called *parallax*. The image

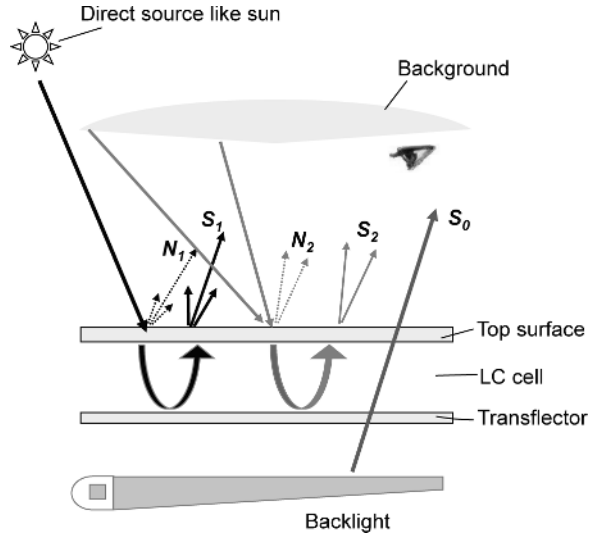

Figure 1.34 Consideration of sunlight readability of a reflective/transflective LCD

overlap results in deterioration of the observed image. To avoid such a parallax problem, the reflector or transflector is required to be formed close to the image pixel.

Ambient contrast ratio is another important concept that needs to be discussed to help us to understand the reflector/transflector design considerations. Figure 1.34 shows a reflective or transflective LCD under ambient lighting. There are two major ambient light sources: the direct light source such as collimated sunlight impinging on the display in a fixed direction, and the light from the background such as the blue sky and the multiple reflections or scattering of sunlight from various objects, which impinges on the display from every direction. From this illustration, two types of major noise source are observed: reflection N_1 from the collimated direct sunlight (assuming the surface is *not* an anti-glare surface), and reflection N_2 from the background light. Here, the reflection N_1 is confined mainly to the specular direction but small amounts of reflection occur at angles away from the exact specular direction. On the other hand, the light for reflection N_2 comes from all directions, thus N_2 may be viewed as uniformly distributed noise. Besides these surface reflections, another type of noise may come from stray ambient light that reaches the eye directly from scattering elsewhere, which is not shown in the figure but which we designate N_0. The direct sunlight and

background intensity vary as the location or time change. Typically, direct sunlight can be greater than 100 000 lux and in full daylight the background may vary from 10 000 lux to 25 000 lux [46]. Such strong ambient light can easily wash out the image from a transmissive display (with a 200-nit surface luminance), even if an anti-reflection coating with $SR < 1\%$ is adopted. For the signals, we have S_1 from the direct light source and S_2 from the background after traversing the LC cell twice. Or, if the backlight of the display is turned on, another signal S_0 contributing from the backlight will also exist. Therefore, the ambient contrast ratio of the display should be defined as $\mathrm{ACR} = (\mathrm{S_0} + \mathrm{S_1} + \mathrm{S_2})/(\mathrm{N_1} + \mathrm{N_2}) + 1$ (please refer to Chapter 6 for more details of this ACR derivation). However, not all the surface reflections of the ambient light will be within the acceptance angle of the eye, and the above equation is just a qualitative expression.

From this analysis, when we discuss the contrast ratio of a display under complex ambient conditions, all these sources of noise must be taken into account. Detailed analysis of display readability will be discussed in a later chapter.

1.5.2 Reflector Designs

The light source and reflection pattern discussed above give rise to some requirements for designing and optimizing a reflective or transflective LCD. Typically, the human eye is located about 30 to 50 cm from the panel surface and is axially within 10° of the surface normal direction. As a result, for high brightness and a wide viewing angle, an ideal reflector or transflector should be able to collect most random incident light and redirect it out to the viewer in a confined cone centered about 10° from the normal direction. For such a case, a reflector with a bumpy surface is preferred. In addition, for good contrast ratio, it should also have the ability to deflect the output light S_1 away from the specular reflection N_1, i.e., the angles of incidence and exit need to be asymmetrical.

A conventional reflector widely used in reflective and transflective LCDs is a diffusive type, in which bumpy structures are formed directly on the flat substrate surface. A dielectric layer is first coated on to a flat substrate, then it is patterned by photolithography to make random bumps (randomness needs to be controlled), and finally a metal layer is coated on to the bumpy surface. This type of bumpy reflector can diffusively reflect the incident light into a wide viewing cone that is much wider than the useful 10° cone for human eyes. Thus, a large amount of incident light is wasted, yielding insufficient useful reflectance and contrast ratio. An alternative method to gain both satisfactory contrast and brightness is to form a diffusive micro

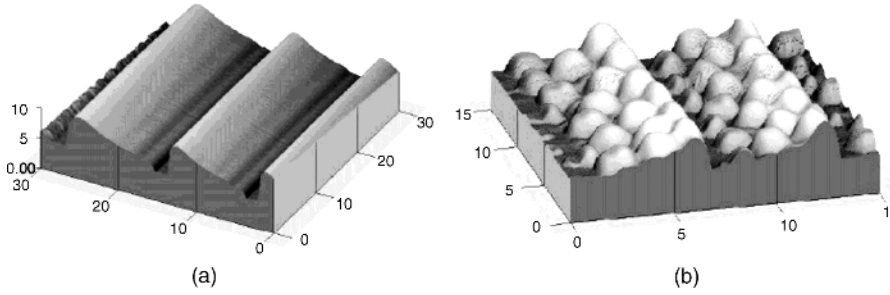

Figure 1.35 (a) A micro slant reflector (MSR) and (b) a diffusive micro slant reflector (DMSR) with a micro bumpy diffusive surface (courtesy of (43) and (44), Reproduced by permission of SID)

slant reflector (DMSR) or transflector, as shown in Figure 1.35 [47, 48]. The DMSR in Figure 1.35(b) can use its bumpy surface to collect random incident light and deflect the output beam away from the major specular reflection direction into the useful viewing cone. Compared with a conventional flat reflector structure, fabricating a DMSR requires more photolithographic steps. For example, first, the photo-resist is exposed by a multi-step exposure method to create the MSR structure in Figure 1.35(a), then a second exposure is used to obtain the bumpy surface profile, and finally a metal such as aluminum is deposited on the surface. The diffusive property is highly related to the second exposure step which controls the height and pitch of the bumps. To cover the entire visible spectrum, multiple bump pitches are required.

In addition to DMSR structures, researchers [49] have recently proposed utilizing multiple ($\sim$25) surface relief micro-gratings combined into one reflector to effectively collect more light from every direction; the diffractive reflector structure and its output pattern are shown in Figure 1.36. As we can see, gratings with different pitch lengths and inclined angles are used to cover the wavelengths in the visible range and to diffract the output light into a cone that is centered on the normal direction. As a result, the major output deviates from the specular reflection and more light is confined to the useful viewing cone. From these simulated results, this structure could improve the reflectance in the normal direction by a factor of 2 compared with the conventional flat bumpy reflectors. However, fabrication might be somewhat complicated.

Another type of reflector of interest is the nano wire grid polarizer (WGP) [50–52]. Figure 1.37 shows the schematic structure of a nano wire

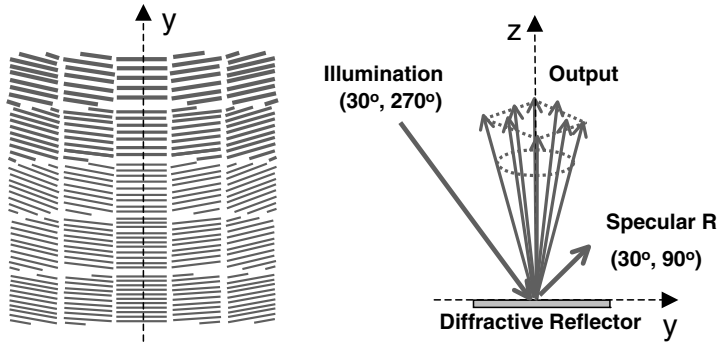

Figure 1.36 Structure and reflective pattern of the diffractive reflector (redrawn from (49))

grid polarizer having metal strips periodically formed on a glass substrate. When the pitch length P is far shorter than the incident wavelength, this metal grating structure functions like a polarization-dependent reflector. For unpolarized light incident on the WGP surface, the wave components with polarization parallel to the metal ribs will excite the unrestricted movement of electrons. The electron movement, in turn, excites a forward traveling wave as well as a backward or reflected wave, with the forward traveling wave canceling exactly the incident wave in the forward direction in the same polarization, yielding a strong reflection for this polarization. In contrast, if the incident wave is polarized perpendicular to the wire grid, the movement of electrons along this direction is restricted and the incident wave has substantial transmission. According to these properties, a wire grid

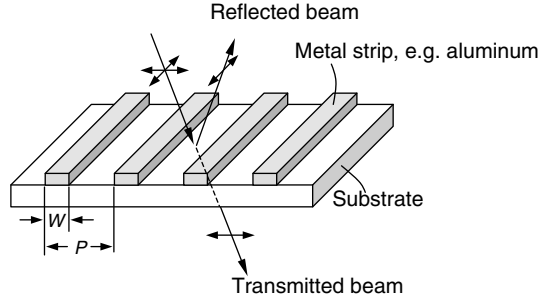

Figure 1.37 Schematic illustration of a nano wire grid polarizer and its characteristics

polarizer can be viewed as a polarization-dependent reflector for reflective and transflective LCDs or a reflective polarizer for the application of backlight recycling. Detailed discussion of the application of nano WGPs in displays will be addressed in Chapter 4.

1.6 Backlight

1.6.1 Backlight Configuration

The backlight configuration is different for a small-panel mobile phone and a large LCD TV. For mobile displays, edge lighting using LEDs is most desirable to achieve the required slim profile. A typical backlight configuration for a mobile display is shown in Figure 1.38(a), where light from edge LEDs is coupled into the light guide plate (LGP) which has patterns on its rear surface enabling light to be scattered towards the LCD cell. A non-metallic reflector with high reflectivity (>95%) is laminated behind the LGP to reflect any light leaving the LGP in a direction away from the LCD. To remove the pattern on the rear LGP surface (which creates hot spots) from the reflected light and make the output more uniform, a diffuser foil is then laminated on the front surface of the LGP. Further, one (oriented in the X or Y direction) or two (one oriented in each of the X and Y directions) prism films such as 3M´s BEF [6] are then attached to collect and collimate off-axis light into a cone within about $\pm 35^{\circ}$ of the normal axial direction. In front of the prism films, there could either be no diffuser, for thickness and cost considerations, or a second diffuser to protect the prism films and reduce the moiré between the periodic structure of the films and pixel arrays. For backlight recycling, a reflective polarizer such as 3M´s DBEF (dual brightness enhancement film) [53] or a wire grid polarizer sheet [50–52] could also be placed before the rear sheet linear polarizer. The function of each different backlight element is illustrated in Figure 1.38(b).

For mobile display applications, low cost, minimum thickness, and high power efficiency from the backlight unit are most critical. To obtain good light efficiency for high brightness, each element, such as the LGP´s extraction factor, needs to be optimized. To reduce the thickness, researchers and engineers attempt to combine one or two prisms, and even the rear diffuser into the LGP structure, but a drawback is fabrication complexity, resulting in a much higher cost. A great deal of optimization work in both optical design and fabrication processes still needs to be conducted in order to perfect these mobile display devices.

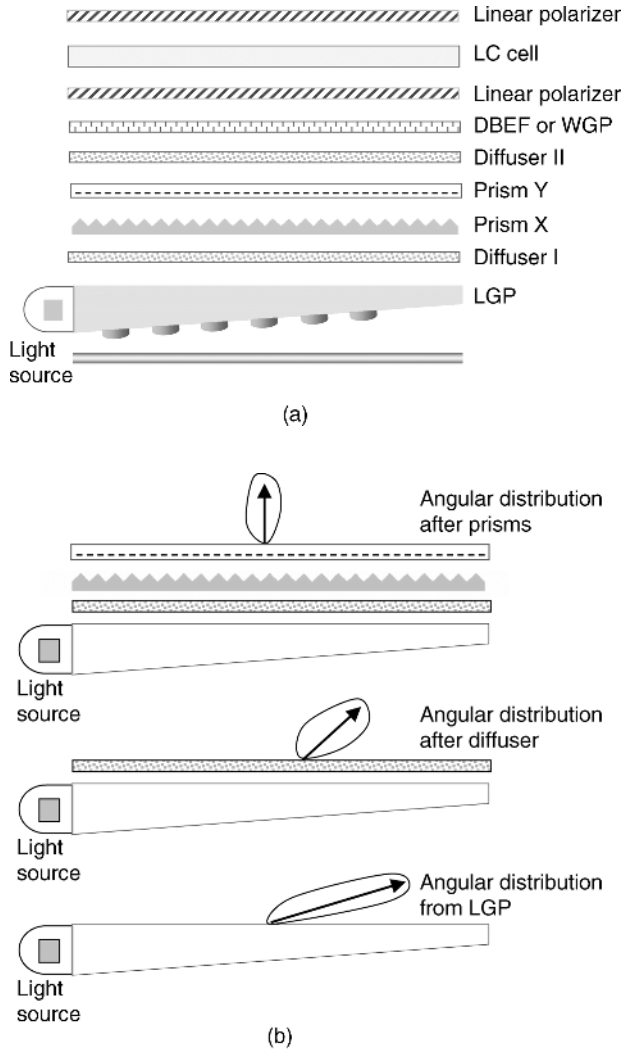

Figure 1.38 (a) Schematic configuration of the backlight unit in a mobile display; (b) angular light profile after each element

1.6.2 CCFL and LED Light Sources

The cold cathode fluorescent lamp (CCFL) is extensively used as a light source for LCDs owing to its ability to produce very bright white light at low cost and high efficiency. The CCFL is a discharge lamp constructed from a

phosphor-coated glass cylinder with a mixture of mercury and a gas such as argon at low pressure sealed inside it with an electrode at either end. When a relatively high voltage is applied to the anode and cathode in the CCFL, a strong electric field is generated to accelerate electrons between the two electrodes. The collision of electrons with the mercury vapor excites mercury atoms above the ground state. Adding a fill gas enhances ionization of the mercury vapor at a lower voltage. Ultraviolet energy is released as excited mercury atoms decay back to the stable ground state, which in turn stimulates the phosphor to emit light in the visible spectrum. To generate white light for display purposes, tri-phosphors with individual red, green, and blue emission are utilized in the phosphor coating. The ratio of these different phosphors determines the output spectrum of the white light.

A typical spectrum of CCFL light is shown in Figure 1.39. As a reference, the spectra of the R, G, and B color filters used in LCDs are also included as dashed lines. The three primary peaks of the CCFL spectrum are located near 435 nm, 545 nm, and 615 nm. The green peak exhibits the narrowest FWHM (full width at half maximum) peak compared with the blue and red ones. However, due to the properties of the phosphors, there are still two undesired secondary peaks located near 490 nm and 585 nm, resulting in poor color

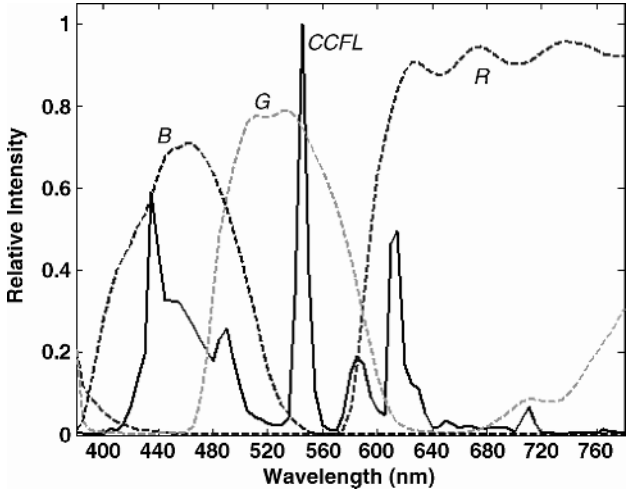

Figure 1.39 Emission spectrum of a CCFL light source (solid line) and the transmission spectra of RGB color filters (dashed lines). Note: the intensity is on a relative scale

separation and a smaller color gamut of about 72% of NTSC (National Television System Committee) in the CIE (International Committee on Illumination) 1931 plot. By shifting both primary and side peaks towards the red and adjusting the relative intensity of each peak by modifying the phosphors to better match the color filter spectrum, more highly saturated green and red colors can be achieved, improving the color extent to about 92% of NTSC [54]. Presently, CCFLs are still widely used for medium-sized and large LCD panels, because of their low cost, good stability, and simple thermal management.

LEDs are another widely used backlight source for LCDs (dominating in small display applications such as cell phones) owing to their compact size and steadily improving brightness. To obtain white light using LEDs, three different methods can be adopted [55]. One method is to mix light from independent R, G, and B LEDs. This method provides a very large color gamut, and is inherently the most efficient. The spectrum obtained by this method is shown in Figure 1.40. Using RGB LEDs enables local dimming to be used, enhancing the dynamic contrast ratio (to $>10^6:1$ under dark room conditions) and reducing power consumption (for DCR characterization, the backlight is underpowered in the dark state, while for a regular static contrast ratio measurement, the backlight is still fully on in the dark state). However, to

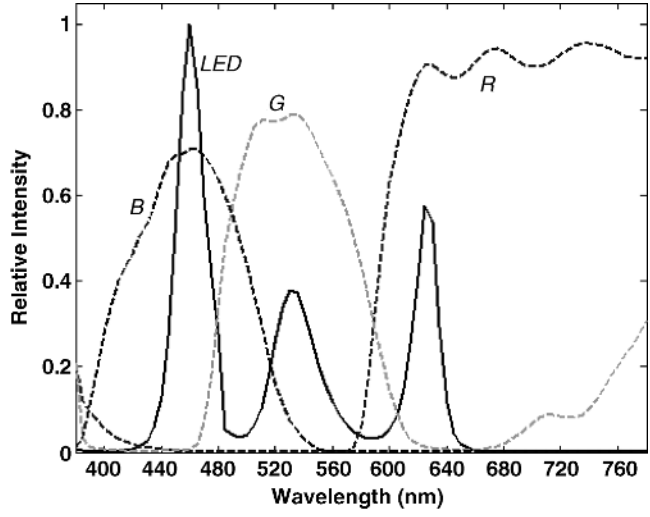

Figure 1.40 Emission spectrum of a white light source using R, G, and B LEDs

accurately stabilize the white point and reduce color shift originating from temperature variation and differential aging of the three colors, complicated driving electronics are needed. In addition, color mixing is not easy, especially in small-panel mobile displays, since the available coupling distance for different colored light is limited. Thus, this method is only used in high-end medium to large LCD panels such as more expensive notebooks and LCD TVs.

A second approach for achieving white light is to use a UV LED to pump R, G, and B phosphors. This method exhibits high color rendering, a stable white point, and a simpler driving circuit. But the efficiency is not good due to the inherent properties of the phosphors. In addition, the variation of the white point with polar angle is large. Moreover, with the existence of the UV LED, more consideration has to be given to the packaging of the backlight in order to avoid degradation from the UV light of other optical elements [55].

A third approach, and the dominant one for small panels, is to use a blue LED (InGaN) to pump a yellow phosphor (YAG). This design converts part of the blue LED light efficiently to a broad spectrum centered at about 580 nm, thus the combination of blue and yellow gives a pseudo white color. The spectrum of this white LED is shown in Figure 1.41. This method is simple and

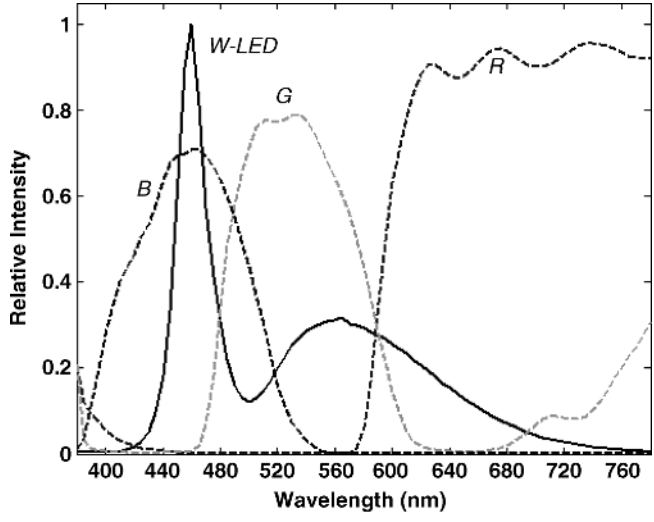

Figure 1.41 Emission spectrum of a white light source using blue LED-pumped yellow phosphor

provides good color rendering, while exhibiting excellent stability and reliability. As with the second approach, the efficiency is limited due to the phosphors. In addition, in practice, both the peak wavelengths of the emissive blue LEDs and the thicknesses of the yellow phosphors have certain variations, resulting in variations in the output white points. Thus, LEDs have to be binned according to their spectral characteristics for users to choose, and manufacturing variations arise as a result of these factors.

When using a white light source, the spectrum must be evaluated in accordance with the transmission spectra of the color filters used in LCDs. To obtain a large color gamut, good separation of the three primary colors is important. Referring to Figures 1.40 and 1.41, the spectrum using three R, G, and B LEDs exhibits the best color separation with the largest color gamut. For the CCFL and W-LED, a smaller color gamut is achievable owing to poor color separation. To improve optical performance characteristics such as luminous efficacy and color gamut, the spectra of the light source and color filters need to be further improved to increase primary color separation and improve green light components to overlap the human eye sensitivity function, centered at about 555 nm.

1.6.3 Other Backlight Elements and Films

In addition to the light source, other optical elements in the backlight unit also play critical roles in directing more light towards the viewer. Referring to the optical configuration shown in Figure 1.38, the element next to the light source is the light guide plate (LGP) that is typically made of polymethyl methacrylate (PMMA) material. The major function of an LGP is to couple out light from the light source and spread it uniformly towards the display or towards the rear reflector to be recycled back into the system. For small mobile displays, the LGP is typically wedge shaped with micro patterns on its rear surface. Optically, the wedge shape will gradually collimate the incident beam towards the normal direction. As a simple illustration, for a wedge-shaped LGP with a smooth surface (Figure 1.42), each reflection on one interface will give a reduction of β in the next incident angle with respect to the new interface normal direction, where β is the wedge angle. After several reflections, the light will exit the LGP, once the incident angle becomes less than the critical angle (determined by the refractive index difference). However, a smooth rear surface of the LGP is not preferred. As we can see, it is possible that some light will exit the LGP through the rear surface, and will be reflected by the reflective sheet. Also, some light will

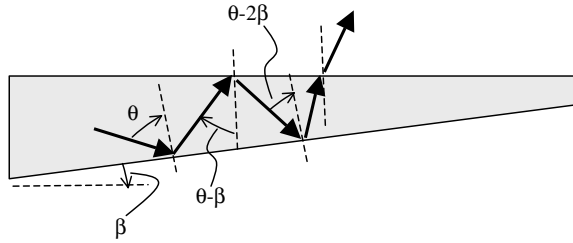

Figure 1.42 Light path in a wedge-shaped LGP with a smooth surface

travel to the right-hand end of the LGP and will be lost. Besides, the light output intensity distribution along the display will not be uniform with a smooth rear surface. To reduce light loss and obscure the output light (to eliminate any possible fixed patterns from the backlight structures before light exits the LGP front surface), certain microstructure patterns need to be formed on the rear LGP surface (as shown in the backlight configuration in Figure 1.38) to scatter (or on the front surface to extract) the incident rays. For low cost, a molding technique with the addition of a chemical etching step or a microstructure method can be employed to form such micro-patterns on the rear LGP surface. The uniformity can be adjusted by the pattern distribution and density. In all, by adjusting the micro-patterns on the LGP surface (dots are sparse near the light source and become denser as they approach the other end), the final output from the LGP will be suitable for further improvement by the optical elements between the LGP and the LCD.

In front of the LGP is a diffuser plate that functions as a means of eliminating images of the rear patterns of the LGP from the reflected light and making the output light more uniform in both a spatial and an angular sense. Typically, several mechanisms and methods are used to diffuse light, as shown in Figure 1.43 [56]. The bulk diffusion method uses a plate made of a bulk material mixed with tiny particles with a small refractive index difference between these two materials. Such a diffuser cannot collimate light. Another method is to engineer non-uniform textures on the exit surface of the diffuser: light collimation can be controlled by forming a particular surface slope distribution. Similarly, spherical beads can also be coated in a random distribution on the exit surface to generate diffusion and control the collimation of the light at the same time. Another interesting method involves the formation of random micro-lenses on a surface as the diffuser, so when the focal length of each micro-lens is small, the exit light from the

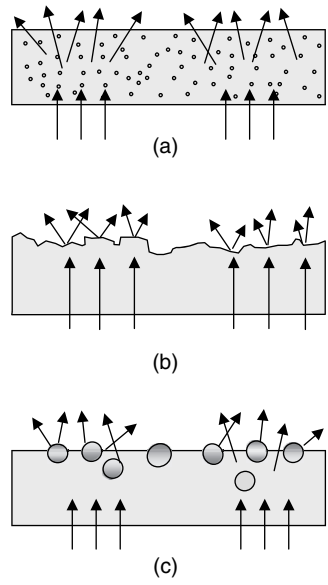

Figure 1.43 Different types of diffusion: (a) bulk diffusion; (b) engineered surface texture; and (c) surface beads (redrawn from (56))

micro-lens will diverge in different directions, creating an effect similar to a diffuser.

After the diffuser plate come the prism films designed to collimate the incident light. A 90° prism structure is shown in Figure 1.44, where the prism

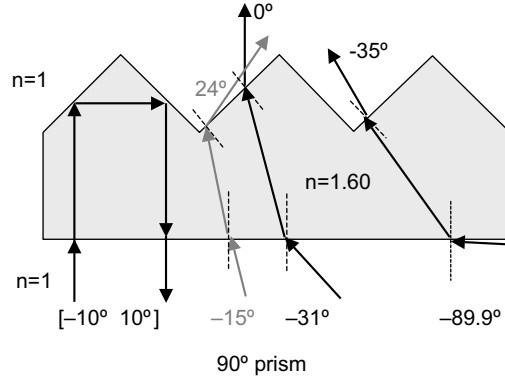

Figure 1.44 Schematic structure of a 90° prism sheet with some typical ray traces

refractive index is 1.60. Therefore the critical angle for an internal reflection is about 38.7°. Several representative rays are shown in the plot to illustrate the prism´s working mechanism. When the incident ray has an angle within 10° of the normal axial direction, the beam will be totally internally reflected back and can be recycled by being bounced back from the reflective sheet and being diffused by other elements. When the incident angle increases, the output ray is transmitted and is refracted over a certain angular range. Besides these typical rays, there are other rays not shown in the plot, for which the optical path is more complicated. In addition, a single prism sheet only confines light in one dimension. A second prism sheet placed perpendicular to the first is needed to collimate the output beam into a cone along the axial direction. As an illustration, the simulated overall light output patterns from the rear LGP and the following two prisms are plotted in Figure 1.45.

Because of the periodic structure of the prism sheet, a moiré pattern, defined as an optical effect resulting from grating beating, might occur [56]. Therefore, a second diffuser sheet which functions also as a protective layer for the BEF films might be employed, which is usually the case in medium- and large-panel LCDs. However, for a small-panel display, because such an optical effect might not be severe and minimizing the thickness of the device is of primary concern, this second diffuser sheet might be omitted.

To further improve the axial light intensity, a reflective polarizer might be placed between the rear linear polarizer and the prism sheet. Presently, the dominating reflective polarizer is 3M´s DBEF film, which is formed by hundreds of dielectric stacks with alternating birefringent and isotropic polymer layers [53]. A detailed structure can be seen in Figure 1.46, where the isotropic layer has $n_x = n_y = n$ and the birefringent layer has $n_x = n < n_y$. Therefore, at normal incidence in the z direction, the incident wave with its polarization along the x-axis always encounters identical refractive index values and can traverse the whole system with high transmission. In contrast, light polarized along the y-axis has alternating high and low refractive indices n_H (~1.88) and n_L (~1.57), resulting in multiple internal reflections and interference effects that, in turn, affect the overall reflection and transmission. In a similar manner to a multi-layered dielectric mirror, by properly adjusting layer thickness to satisfy the Bragg condition, a reflection band with high reflectivity can be obtained. The central peak wavelength is related to the product of the thickness and refractive index of each layer. Typically, bandwidth is determined by the refractive index difference between layers. A larger refractive index difference would provide a wider reflection band

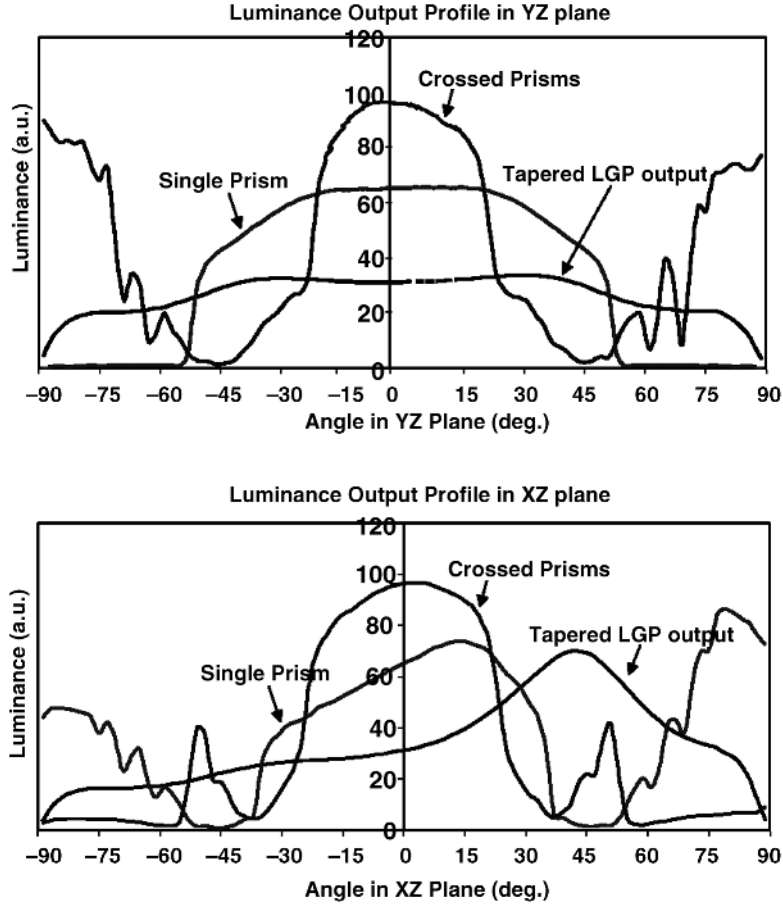

Figure 1.45 Light profile after passing the LGP and prisms (from Lighttool simulations)

and a high reflection peak within the band. To achieve a broadband DBEF film, we can laminate multiple stacks with each stack centered at a different wavelength and with a linear gradient in layer thickness [57]. With hundreds of stacks, reflectance greater than 95% can easily be obtained at normal incidence. A DBEF using multiple stacked units with a birefringent layer and an isotropic layer is quite different in its off-axis performance from a multi-layered dielectric mirror using only isotropic materials with alternating

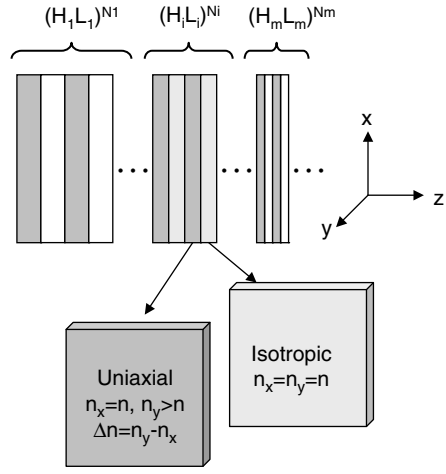

Figure 1.46 Schematic configuration of DBEF film using multiple polymeric layers

low and high refractive indices. In the multi-layered dielectric mirror, the reflection falls quickly as the incident angle departs from the normal direction, which is the Brewster effect. In the DBEF, by properly setting the n_y and n_z value for each layer, the Brewster angle for the polarization along the *y*-axis can be tuned to be imaginary, thus a high off-axis reflection can also be achieved [53].

Another type of reflective polarizer of interest is the nano wire grid polarizer (WGP) as illustrated in Figure 1.37 and discussed earlier in this chapter. Presently, this technology is still under development for mass production, because very narrow grid width and spacing (less than 100 nm) need to be controlled. Currently, the major fabrication methods for nano WGPs are conventional lithography, conventional nano-imprint [58, 59], roll-to-roll nano-imprint lithography (R2RNIL), and embossing [60], among which the R2RNIL method shows great potential for reducing the cost of nano WGPs.

For mobile displays, achieving minimum thickness is one of the primary requirements. To reduce the backlight unit thickness, one trend is to combine multiple film technologies into a single optical element, such as combining the prism structures into the LGP, making the bulk of the LGP a diffuser, or creating prism structures on the DBEF films [61]. Many new configurations

have been developed or are under development, providing many opportunities in research, development, and business.

1.7 Summary

In this chapter, the background of transflective LCD technology has been briefly addressed. The basic device configurations and working mechanisms of the major optical elements in an LCD device, such as polarizers, LC molecular alignment, compensation films, reflectors, and backlight units, have been briefly reviewed. More detailed description of some specific topics will be provided in later chapters. This chapter not only serves as a basis for readers to understand the working principles and design concepts of a practical transflective LCD, but also paves the way for optimizing these display devices.

References

[1] Wu, S.T. and Wu, C.S. (1996) Mixed-mode twisted nematic liquid crystal cells for reflective displays. *Appl. Phys. Lett.*, **68**, 1455–1457.
[2] Wu, S.T. and Yang, D.K. (2001) *Reflective Liquid Crystal Displays*. John Wiley & Sons, Inc., New York.
[3] de Gennes, P.G. and Prost, J. (1993) *The Physics of Liquid Crystals*, 2nd edition. Clarendon Press. Oxford.
[4] Yang, D.K. and Wu, S.T. (2006) *Fundamentals of Liquid Crystal Devices*. John Wiley & Sons, Ltd, Chichester.
[5] Zhu, X., Ge, Z., Wu, T.X. and Wu, S.T. (2005) Transflective liquid crystal displays. *J. Disp. Technol.*, **1**, 15–29.
[6] For example, see BEF film from http://www.3m.com/.
[7] Takeda, A., Kataoka, S., Sasaki, T., Chida, H., Tsuda, H., Ohmuro, K., Sasabayashi, T., Koike, Y. and Okamoto, K. (1998) A super-high image quality multi-domain vertical alignment LCD by new rubbing-less technology. *SID Tech. Digest*, **29**, 1077–1080.
[8] Tanaka, Y., Taniguchi, Y., Sasaki, T., Takeda, A., Koibe, Y. and Okamoto, K. (1999) A New Design to Improve Performance and Simplify the Manufacturing Process of High-Quality MVA TFT-LCD Panels. *SID Tech. Digest*, **30**, 206–209.
[9] Kataoka, S., Takeda, A., Tsuda, H., Koike, Y., Inoue, H., Fujikawa, T., Sasabayashi, T. and Okamoto, K. (2001) A New MVA-LCD with Jagged Shaped Pixel Electrodes. *SID Tech. Digest*, **32**, 1066–1069.

[10] Schadt, M. and Helfrich, W. (1971) Voltage-dependent optical activity of a twisted nematic liquid crystal. *Appl. Phys. Lett.*, **18**, 127.
[11] Soref, R.A. (1974) Field effects in nematic liquid crystals obtained with interdigital electrodes. *J. Appl. Phys.*, **45**, 5466.
[12] Ohe, M. and Kondo, K. (1995) Electro-optical characteristics and switching behavior of the in-plane switching mode. *Appl. Phys. Lett.*, **67**, 3895.
[13] Lee, S.H., Lee, S.L. and Kim, H.Y. (1998) Electro-optic characteristics and switching principle of a nematic liquid crystal cell controlled by fringe-field switching. *Appl. Phys. Lett.*, **73**, 2881.
[14] Bos, P.J. and Koehler-Beran, K.R. (1984) The pi-cell: a fast liquid-crystal optical-switching device. *Mol. Cryst. Liq. Cryst.*, **113**, 329.
[15] Yamaguchi, Y., Miyashita, T. and Uchida, T. (1993) Wide-viewing-angle display mode for the active-matrix LCD using bend-alignment liquid-crystal cell. *SID Tech. Digest*, **24**, 273–276.
[16] Kim, K.H., Lee, K.H., Park, S.B., Song, J.K., Kim, S.N. and Souk, J.H. (1998) Domain divided vertical alignment mode with optimized fringe field effect. In Proc. 18th Int. Display Research Conf. (Asia Display ´98), pp. 383–386.
[17] Fujimura, Y., Kamijo, T. and Yoshimi, H. (2003) Improvement of optical films for high performance LCDs. *Proceedings of SPIE*, **5003**, 96–105.
[18] Yang, Y.-C. and Yang, D.K. (2008) Achromatic reduction of off-axis light leakage in LCDs by self-compensated phase retardation (SPR) film. *SID Tech. Digest*, **39**, 1955–1958.
[19] McKnight, W.H. Stotts L.B. and Monahan M.A. (1982) Transmissive and Reflective Liquid Crystal Display. U. S. Patent 4 315 258 (February 9, 1982).
[20] Yoshida, H., Tasaka, Y., Tanaka, Y., Sukenori, H., Koike, Y. and Okamoto, K. (2004) MVA LCD for Notebook or Mobile PCs with High Transmittance, High Contrast Ratio, and Wide Angle Viewing. *SID Tech. Digest*, **35**, 6–9.
[21] Pancharatnam, S. (1956) Achromatic combinations of birefringent plates. *Proc. Ind. Acad. Sci. A*, **41**, 130–144.
[22] Khoo, I.C. and Wu, S.T. (1993) *Optics and Nonlinear Optics of Liquid Crystals*. World Scientific, Singapore.
[23] Zhu, X., Ge, Z. and Wu, S.T. (2006) Analytical solutions for uniaxial-film-compensated wide-view liquid crystal displays. *J. Disp. Technol.*, **2**, 2–20.
[24] Bigelow, J.E. and Kashnow, R.A. (1977) Poincaré sphere analysis of liquid crystal optics. *Appl. Opt.*, **16**, 2090.
[25] Cognard, J. (1982) Alignment of nematic liquid crystals and their mixtures. *Mol. Cryst. Liq. Cryst., Suppl.*, **1**, 1.
[26] Mori, H. (2005) The wide view film for enhancing the field of view of LCDs. *J. Disp. Technol.*, **1**, 179.
[27] Takeuchi, K., Yasuda, S., Oikawa, T., Mori, H. and Mihayashi, K. (2006) Novel VW film for wide-viewing-angle TN-mode LCDs. *SID Tech. Digest*, **37**, 1531–1534.

[28] Lien, S.C. and John, R.A. (1994) Liquid Crystal Displays Having Multi-Domain Cells. U. S. Patent 5 309 264. (May 1994).
[29] Lien, A. and John, R.A. (1993) Multi-Domain Homeotropic Liquid Crystal Display for Active Matrix Application. EuroDisplay ´93, p. 21.
[30] Lien, S.-C.A., Cai, C., Nunes, R.W., John, R.A., Galligan, E.A., Colgan, E. and Wilson, W.S. (1998) Multi-domain homeotropic liquid crystal display based on ridge and fringe field structure. *Jpn J. Appl. Phys.*, **37**, L597.
[31] Song, J.-K., Lee, K.-E., Chang, H.-S., Hong, S.-M., Jun, M.-B., Park, B.-Y., Seomun, S.-S., Kim, K.-H. and Kim, S.-S. (2004) DCCII: Novel method for fast response time in PVA mode. *SID Tech. Digest*, **35**, 1344–1347.
[32] Hanaoka, K., Nakanishi, Y., Inoue, Y., Tanuma, S. and Koike, Y. (2004) A New MVA-LCD by Polymer Sustained Alignment Technology. *SID Tech. Digest*, **35**, 1200–1203.
[33] Kim, S.G., Kim, S.M., Kim, Y.S., Lee, H.K., Lee, S.H., Lee, G.-D., Lyu, J.-J. and Kim, K.H. (2007) Stabilization of the liquid crystal director in the patterned vertical alignment mode through formation of pretilt angle by reactive mesogen. *Appl. Phys. Lett.*, **90**, 261910–261912.
[34] Matsumoto, S., Kawamoto, M. and Mizunoya, K. (1976) Field-induced deformation of hybrid-aligned nematic liquid crystals: new multicolor liquid crystal display. *J. Appl. Phys.*, **47**, 3842.
[35] Hosaki, K., Uesaka, T., Nishimura, S. and Mazaki, H. (2006) Comparison of viewing angle performance of TN-LCD and ECB-LCD using hybrid-aligned nematic compensators. *SID Tech. Digest*, **37**, 721–724.
[36] Uesaka, T., Ikeda, S., Nishimura, S. and Mazaki, H. (2007) Viewing-angle compensation of TN- and ECB-LCD modes by using a rod-like liquid crystalline polymer film. *SID Tech. Digest*, **38**, 1555–1558.
[37] Yeung, F.S., Ho, J.Y., Li, Y.W., Xie, F.C., Tsui, O.K., Sheng, P. and Kwok, H.S. (2006) Variable liquid crystal pretilt angles by nanostructured surfaces. *Appl. Phys. Lett.*, **88**, 051910.
[38] Ito, Y., Matsubara, R., Nakamura, R., Nagai, M., Nakamura, S., Mori, H. and Mihayashi, K. (2005) OCB-WV film for fast-response-time and wide-viewing-angle LCD-TVs. *SID Tech. Digest*, **36**, 986–989.
[39] Lien, A. (1990) Extended Jones matrix representation for the twisted nematic liquid-crystal display at oblique incidence. *Appl. Phys. Lett.*, **57**, 2767–2769.
[40] Yeh, P. and Gu, C. (1999) *Optics of Liquid Crystal Displays*. John Wiley & Sons, Inc., New York.
[41] Ge, Z., Wu, T.X., Zhu, X. and Wu, S.T. (2005) Reflective liquid crystal displays with asymmetric incidence and exit angles. *J. Opt. Soc. Am. A.*, **22**, 966–977.
[42] Fujimura, Y., Nagatsuka, T., Yoshimi, H., Umemoto, S. and Shimomura, T. (1992) Optical properties of retardation film. *SID Tech. Digest*, **23**, 397–400.

[43] Chen, J., Chang, K.C., Delpico, J., Seiberle, H. and Schadt, M. (1999) Wide Viewing Angle Photoaligned Plastic Films For TNLCD. *SID Tech. Digest*, **30**, 98–101.
[44] Nishimura, S. and Mazaki, H. (2003) Viewing angle compensation of various LCD modes by using a liquid crystalline polymer film 'Nisseki LC film'. *Proceedings of SPIE*, **6332**, 633203–1.
[45] Palto, S., Kasianova, I., Kharatiyan, E., Kuzmin, V., Lazarev, A. and Lazarev, P. (2007) Thin coatable birefringent films and their application to VA and IPS mode LCDs. *SID Tech. Digest*, **38**, 1563–1566.
[46] http://en.wikipedia.org/wiki/Daylight.
[47] Ting, D.-L., Chang, W.-C., Liu, C.-Y., Shiu, J.-W., Wen, C.-J., Chao, C.-H., Chuang, L.-S. and Chang, C.-C. (1999) A High Brightness and High Contrast Reflective LCD with Micro Slant Reflector (MSR). *SID Tech. Digest*, **30**, 954–957.
[48] Wen, C.-J., Ting, D.-L., Chen, C.-Y., Chuang L.-S. and Chang C.-C. (2000) Optical Properties of Reflective LCD with Diffusive Micro Slant Reflector (DMSR). *SID Tech. Digest*, **31**, 526–529.
[49] Kim, J.H., Yu, J.-H., Cheong, B.-H., Choi, Y.-S. and Choi, H.-Y. (2008) Highly efficient diffractive reflector using micrograting for reflective display. *Appl. Phys. Lett*., **93**, 041915.
[50] Perkins, R.T., Hansen, D.P., Gardner, E.W., Thorne, J.M. and Robbins, A.A. (2000) Broadband wire grid polarizer for the visible spectrum. U. S. Patent 6 122 103 (September 2000).
[51] Yu, X.J. and Kwok, H.S. (2003) Optical wire-grid polarizers at oblique angles of incidence. *J. Appl. Phys.*, **93**, 4407–4412.
[52] Ge, Z. and Wu, S.T. (2008) Nano-wire grid polarizer for energy efficient and wide-view liquid crystal displays. *Appl. Phys. Lett*., **93**, 121104.
[53] Weber, M.F., Stover, C.A., Gilbert, L.R., Nevitt, T.J. and Ouderkirk, A.J. (2000) Giant Birefringent Optics in Multilayer Polymer Mirrors. *Science*, **287** (5462), 2451–2456.
[54] Kim, S.S., Berkeley, B.H. and Kim, T. (2006) Advancements for highest-performance LCD-TV. *SID Tech. Digest*, **37**, 1938–1941.
[55] Scott, K. (2004) *From concept to reality to the future*. Educational presentation for the IESNA Great Lakes Region, June,
[56] Graf, J., Olczak, G., Yamada, M., Colyle, D. and Yeung, S. (2007) Backlight film & sheet technologies for LCDs. SID seminar M-12. May, 21.
[57] Li, Y., Wu, T.X. and Wu, S.T. (2009) Design optimization of reflective polarizers for LCD backlight recycling. *J. Disp. Technol.*, **5**, 335–340.
[58] Wang, J., Walters, F., Liu, X., Sciortino, P. and Deng, X. (2007) High-performance, large area, deep ultraviolet to infrared polarizers based on 40 nm line/78 nm space nanowire grids. *Appl. Phys. Lett*., **90**, 061104.
[59] Wang, J., Chen, L., Liu, X., Sciortino, P., Liu, F., Walters, F. and Deng, X. (2006) 30-nm-wide aluminum nanowire grid for ultrahigh contrast and

transmittance polarizers made by UV-nanoimprint lithography. *Appl. Phys. Lett.*, **89**, 141105.

[60] Ahn, S.H., Kim, J.-S. and Guo, L.J. (2007) Bilayer metal wire-grid polarizer fabricated by roll-to-roll nanoimprint lithography on flexible plastic substrate. *J. Vac. Sci. Technol. B.*, **25** (6), 2388.

[61] Kalantar, K. (2006) *LCD Backlighting*. SID Application Tutorial Notes, A-5, San Francisco, June.